NASA Contractor Report 4371

Testing of Transition-Region
Models: Test Cases and Data

Bart A. Singer, Surya P. G. Dinavahi,
and Venkit Iyer
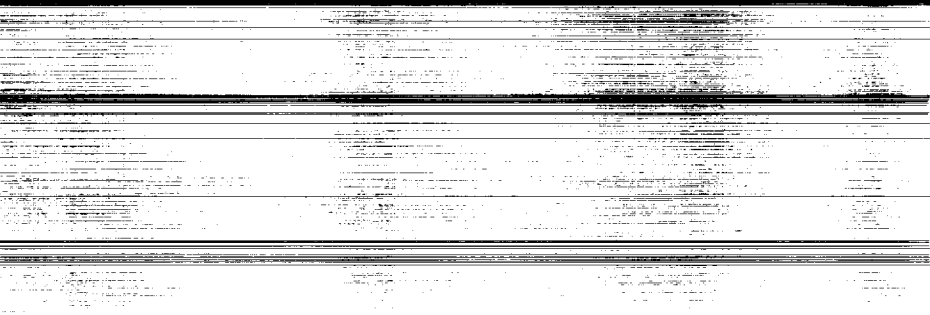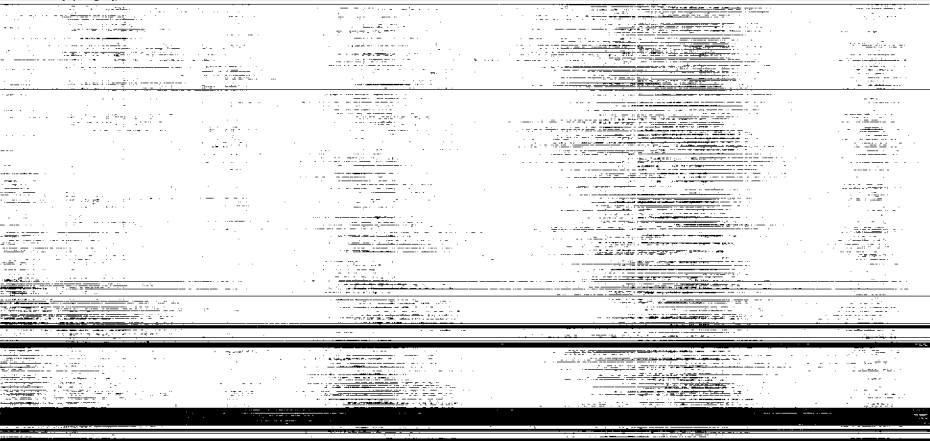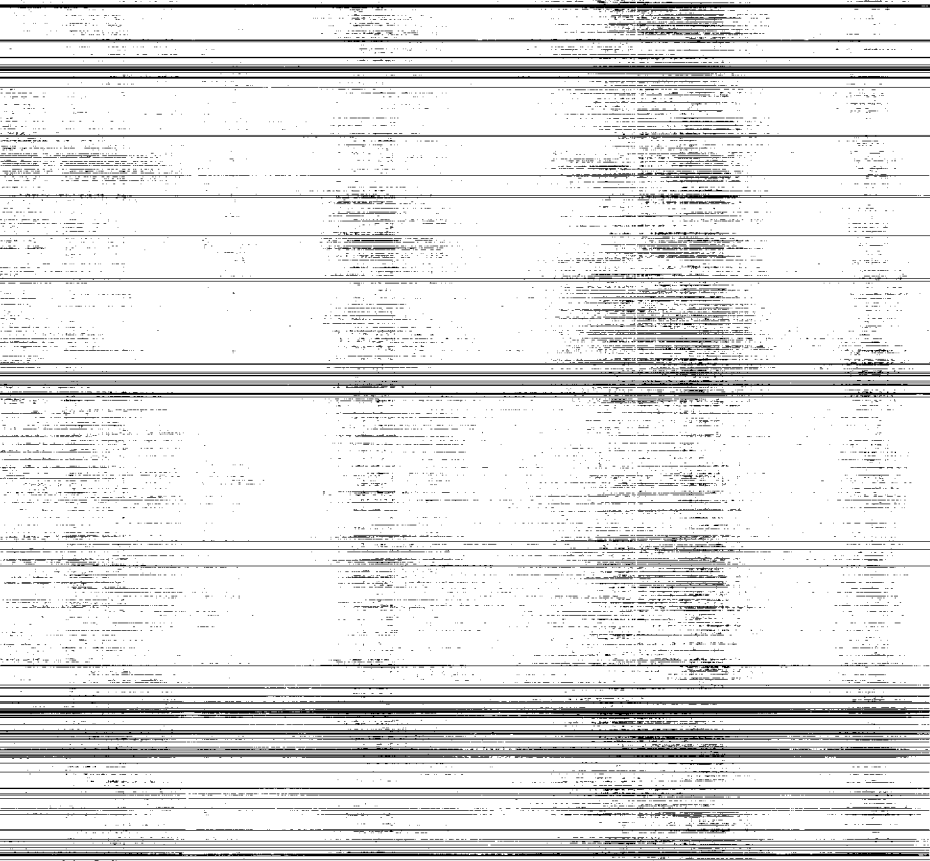
NASA Contractor Report 4371

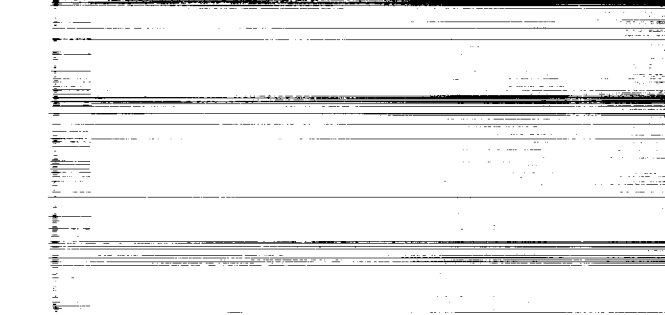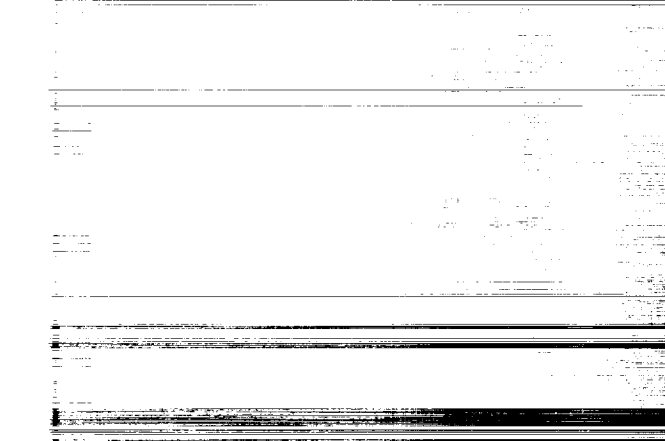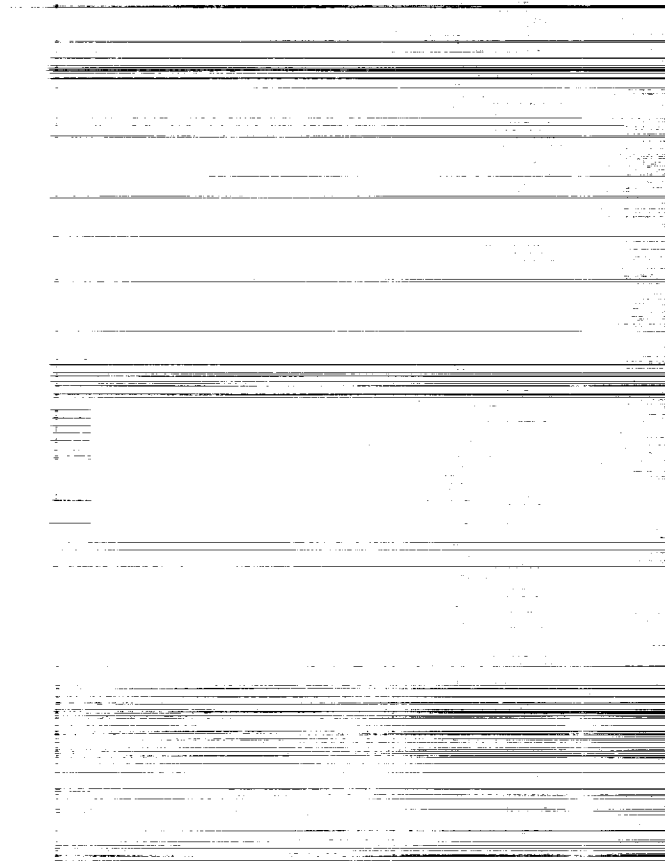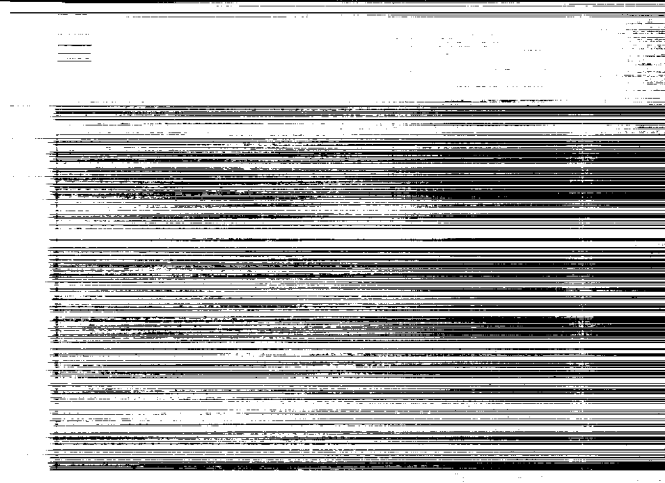# Testing of Transition-Region Models: Test Cases and Data

Bart A. Singer
High Technology Corporation
Hampton, Virginia

Surya P. G. Dinavahi
Analytical Services & Materials, Inc.
Hampton, Virginia

Venkit Iyer
ViGYAN, Inc.
Hampton, Virginia

NASA

National Aeronautics and
Space Administration

Office of Management

Scientific and Technical
Information Division

1991

1 Introduction

The laminar-turbulent-transition zone presents special problems for the calculation of boundary-layer flows. Mean-flow quantities obey neither the fully laminar nor the fully turbulent correlations. In addition, local maxima in skin friction, wall temperature and heat transfer often occur near the end of the transition region. Traditionally, modeling this region has been important for the design of turbine blades, where the transition region is long relative to the chord of the blade. More recently, the need for better transition-region models has been recognized by designers of hypersonic vehicles. Here the high Mach number, the low Reynolds number, and the low-disturbance flight environment emphasize the importance of the transition region. While numerous models have been proposed for the calculation of mean-flow quantities through the transition region, the models are rarely tested over the full range of flows for which they may be used. The proponents of a model typically present results for flows which are similar to the ones from which the model was calibrated. These tests show how well the model can perform, but do not show the model's limitations.

The purpose of this report is to document the results obtained from different transitional-flow models for a wide variety of flows. Since the transitional-flow models depend on having a satisfactory turbulence model, the turbulence models are first tested for several fully turbulent flows. In Section 2 we briefly discuss the turbulent and transition-region models. Detailed descriptions of

the flows used and the results obtained with the various models are given in
Section 3. We summarize our work in Section 4.

2   The Models

2.1   Turbulence Models

We consider two common algebraic turbulence models in their fully turbulent
forms. Transitional-flow effects will be considered later. The first is the
Baldwin-Lomax model [1]; the other is a variation of the Cebeci-Smith [2]
model (The variation that we use is quite similar to that in [3].). In the
models algebraic expressions are used to determine an eddy viscosity, μ_t,
which is added to the molecular viscosity. It is also used, along with a
constant turbulent Prandtl number, $Pr_t = 0.89$, and the specific heat at
constant pressure, c_p, to find an eddy conductivity $k_t = \mu_t c_p / Pr_t$ which is
added to the molecular conductivity.

In describing the models, the streamwise direction is denoted by x, the
wall-normal distance by y, the streamwise velocity by U, and the density by
ρ. A subscript w indicates a wall quantity and an e indicates a boundary-
layer-edge quantity. Both models contain inner and outer layers, hence,

$$\mu_t = \begin{cases} (\mu_t)_{in} & y \le y_c \\ (\mu_t)_{out} & y_c < y \end{cases} \qquad (1)$$

where y_c is the smallest value of y for which $(\mu_t)_{in} = (\mu_t)_{out}$.

The inner regions of both models are similar; the general form is given

by:

$$(\mu_t)_{in} = \rho l^2 |\omega| \tag{2}$$

where

$$l = \kappa y \left[1 - \exp \left(-y/A \right) \right]. \tag{3}$$

In the Baldwin-Lomax model, ω is the vorticity, though for the boundary-layer flows that we are considering, and for the Cebeci-Smith model in general, the approximation,

$$\omega \approx dU/dy \tag{4}$$

is used. The damping coefficient A can be written as

$$A = A^+ \mu/(\rho U_\tau \mathcal{N}) \tag{5}$$

where $U_\tau = \sqrt{(\tau_w/\rho)}$ is the friction velocity and τ_w is the wall shear stress. In the Baldwin-Lomax model, $\mathcal{N} = 1$, while in the Cebeci-Smith model, with no mass transfer at the wall,

$$\mathcal{N} = \left(1 - 11.8 p^+ \right)^{1/2} \tag{6}$$

where

$$p^+ = -\mu_e U_e/(\rho_e U_\tau^3) dU_e/dx. \tag{7}$$

With excessive adverse pressure gradients, $\mathcal{N}$ might not be real. This is not a problem for any of our flows. The value of the von Karman constant, κ, used in the Baldwin-Lomax model is 0.4, while in the Cebeci-Smith model it is 0.41. Both models use $A^+ = 26$. Additional corrections suggested by Cebeci

3

and Smith [2] regarding streamwise and transverse curvature are not required because of the relatively thin boundary layers in the flows considered.

In the outer region, the two models vary more significantly. For Cebeci-Smith,

$$(\mu_t)_{out} = \rho\alpha\bar{\gamma}\left|\int_0^\infty (U_e - U)dy\right| \tag{8}$$

where

$$\alpha = 0.0168\left[1.55/(1 + II)\right] \tag{9}$$

with

$$II = 0.55\left[1 - \exp\left(-0.243z_1^{1/2} - 0.298z_1\right)\right] \tag{10}$$

and

$$z_1 = (Re_\theta/425 - 1). \tag{11}$$

Re_θ is the Reynolds number based on momentum thickness. For values of Re_θ greater than 5000, $\alpha = 0.0168$ is recommended. The quantity $\bar{\gamma}$ is an edge intermittency factor that smoothly reduces the eddy viscosity to zero in the outer part of the boundary layer. The form that we use is the same as that used in [4] and is given by:

$$\bar{\gamma} = \frac{1 - \mathrm{erf}\left[5.0\left(y/\delta - 0.78\right)\right]}{2} \tag{12}$$

where erf is the error function and δ is the boundary-layer thickness based on 99% of U_e.

4

The Baldwin-Lomax model has an outer-region eddy-viscosity relation that can be written as

$$(\mu_t)_{out} = 0.0168 \ \rho C_{cp} F_{wake} F_{Kleb}(y). \tag{13}$$

The constant C_{cp} is 1.6 and

$$F_{wake} = \min \left[y_{max} F_{max}, C_{wk} y_{max} u_{dif}^2 / F_{max} \right]. \tag{14}$$

For boundary-layer flows, y_{max} and F_{max} are determined from

$$F(y) = y|\omega|[1 - \exp(-y/A)] \tag{15}$$

where A is the same as defined for the inner region. F_{max} is the maximum value of $F(y)$ and y_{max} is the value of y at which it occurs. The quantity u_{dif} is the difference between the maximum and minimum total velocities in the profile at a given x location. The constant C_{wk} is 0.25. The Klebanoff intermittency factor is given as

$$F_{Kleb}(y) = \left[1 + 5.5 \left(C_{Kleb} \ y/y_{max} \right)^6 \right]^{-1} \tag{16}$$

where $C_{Kleb} = 0.3$. Further explanations regarding the turbulence models can be found in the original sources.

2.2 Transition-Region Models

Two different transition models are considered here. In implementing the models, we assume that the location at which transition begins is known.

The models are expected to predict the evolution of the velocity, temperature, and density profiles throughout the transition region.

Linear Combination Model

We first consider the linear-combination model proposed by Dey and Narasimha [5]. In linear-combination models the mean flow in the transition region is a linear combination of the mean flows in the laminar and fully turbulent boundary layers. The intermittency is used to obtain the appropriate proportions for the linear combination. Transition starts at the first point, x_t, at which the intermittency is nonzero. This point coincides with the origin of the turbulent boundary layer. The intermittency is given by:

$$\gamma = 1 - \exp\left(-0.411(x - x_t)^2/\lambda^2\right) \qquad (17)$$

where λ is the streamwise distance between the points where $\gamma = 0.25$ and $\gamma = 0.75$. Since λ is not known *a priori*, it is calculated from:

$$\lambda = \left(0.411 Re_\theta^3/N_2\right)^{1/2} \nu/U(x_{t2}) \qquad (18)$$

where ν is the kinematic viscosity at the edge of the boundary layer, $U(x_{t2})$ is the boundary-layer-edge velocity at x_{t2}, and Re_θ is the Reynolds number based on laminar momentum thickness at the point x_{t2}. For mild pressure gradients, $x_{t2} = x_t$. For stronger pressure gradients x_{t2} must be determined from the intermittency distribution itself. We wish to use the model to predict the intermittency distribution and, since there currently is not a correlation for finding x_{t2}, we take $x_{t2} = x_t$. The factor N_2 is a nondimensional

turbulent-spot-formation rate and is determined via the correlation:

$$N_2 = N_0(M, q) + 0.24 L_{t2}^2 \qquad \text{for } L_{t2} > 0 \qquad (19)$$

or

$$N_2 = N_0(M, q) - 323 L_{t2}^3 \qquad \text{for } L_{t2} < 0 \qquad (20)$$

where $N_0 = 0.7 \times 10^{-3}$ for incompressible flows with free-stream turbulence levels, q, greater than 0.2%, and $L_{t2} = \frac{dU_e}{dx} \theta_L^2 / \nu$ is a pressure gradient parameter. Both the free-stream-velocity gradient, $\frac{dU_e}{dx}$, and the laminar momentum thickness, θ_L, are measured at x_{t2}. For compressible flows, the Mach number correction to N_0 given by Narasimha [6] is used. Very low free-stream-turbulence levels require a modified value of N_0. Our modification,

$$N_0 = -1.453 \times 10^{-3} \log q - 1.61 \times 10^{-3} \qquad \text{for } q < 0.2\% \qquad (21)$$

where q is the free-stream-turbulence level in percent, comes from fitting a curve to the data in Figure 5.10 of Dey and Narasimha [5]. To compute the turbulent flow field, the Cebeci-Smith model [2, 3] has been used.

Algebraic Model

The next model we consider is an algebraic model developed at ONERA/CERT and discussed briefly by Arnal [7, 8]. Algebraic models calculate the mean flow from a set of averaged equations in which the effective viscosity, μ_{eff}, is equal to the sum of the molecular viscosity, μ_{mol}, and the product of a transition function, ϵ_t, with a turbulent-eddy viscosity, μ_t, such

that:

$$\mu_{eff} = \mu_{mol} + \epsilon_t \, \mu_t. \tag{22}$$

As with the previous model, μ_t is determined via the Cebeci-Smith model [2, 3]. The transition function, ϵ_t, is **not** the intermittency of the flow, but is an empirically determined expression which governs the relative amounts of molecular to turbulent-eddy viscosity; ϵ_t is a function of

$$\chi_1 = \left(\theta/\theta_t - 1 + 0.005M_e^2\right) / \left(1 + 0.02M_e^2\right), \tag{23}$$

where θ is the momentum thickness of the boundary layer, θ_t is the momentum thickness at the point where the model is started, and M_e is the Mach number at the edge of the boundary layer. The expression for ϵ_t is piecewise continuous in the streamwise direction and is constant across the boundary layer. The algebraic expressions for ϵ_t used in this work are given by Arnal (private communication).

For $0 < \chi_1 \le 0.25$,

$$\epsilon_t = 1 - \exp\left(-4.5\left(\chi_1\left(1 + 0.02M_e^2\right) - 0.005M_e^2\right)^2\right). \tag{24}$$

For $0.25 < \chi_1 \le 0.75$,

$$\epsilon_t = 18.628\chi_1^4 - 55.388\chi_1^3 + 52.369\chi_1^2 - 16.501\chi_1 + 1.893. \tag{25}$$

For $0.75 < \chi_1 \le 3$,

$$\epsilon_t = 1.25 - 0.25\sin\left(\pi\left(0.444\chi_1 - 0.833\right)\right). \tag{26}$$

8

For $\chi_1 > 3$,

$$\epsilon_t = 1. \tag{27}$$

Note that the transition function exceeds unity for part of the region and hence cannot represent the true intermittency of the flow.

The models are implemented in the three-dimensional-boundary-layer code of Iyer [9]. This code is fourth-order accurate in the wall-normal direction and second-order accurate in the stream-surface directions. Numerous examples are given in [9] to verify the accuracy and robustness of the code. Of particular interest to us are the examples of flows over flat plates, cones, and spheroids. The flows that we will consider below are variations on these basic geometries, for which the code has already proven itself capable of computing accurately.

In addition to the boundary-layer code, TRANZ3, an incompressible momentum integral code written by Dey and Narasimha [5] was used to double check many of the low speed results. Details regarding this code are given in [5].

3   Case Description and Results

Four reference quantities are used in the specification of each case: the reference length, L_{ref}; Mach number, M_{ref}; temperature, T_{ref}; and pressure, P_{ref}. The reference velocity, U_{ref}, is calculated. In cases where all the reference quantities are not available, reasonable estimates for the quantities are

9

given. (e.g. For low speed flows the pressure is rarely provided; atmospheric pressure at sea level is used.) Also required for the calculation of each case is the streamwise distribution of edge velocity U_e, and, depending on the boundary conditions, either wall heat flux, q_w, or wall temperature, T_w.

3.1 Fully Turbulent-Flow Cases

The purpose of these cases is to verify that the turbulence models used in this work give satisfactory results for the types of flows we wish to study. Five low-speed, fully-turbulent flows from the 1968 Stanford Conference [10] are studied. Each flow is on a flat plate but involves a different pressure gradient distribution. Flow identification numbers correspond to those used in [10]. The first two flows, ID 1100 and ID 1200, are in adverse pressure gradients. The third flow, ID 1300, is in a favorable pressure gradient and the fourth flow, ID 1400, has zero pressure gradient. In the last case, ID 3300, the turbulent boundary layer starts with a zero pressure gradient. The boundary layer is then suddenly subjected to a strong adverse pressure gradient which is smoothly relaxed. In the discussion of each of these cases the original authors are appropriately cited. However, much of the tabulated data were provided by the authors to the conference organizers and do not appear in the original publications. One supersonic flow case without experimental verification is discussed at the end of this subsection.

Comparisons of the skin-friction coefficient are used to evaluate the mod-

els. The skin-friction coefficient is defined as:

$$C_f = \frac{\tau_w}{1/2\rho_e U_e^2}.$$ (28)

In the 1968 Stanford Conference, two, or sometimes three different estimates of the skin-friction coefficient are given. The symbol C_f is used for the skin-friction coefficient as defined above, where τ_w is determined by a fit of the data to the law of the wall. When the velocity profile in the log layer is accurately measured, we feel that C_f is the most reliable of the three estimates. The quantity C_{fe}, when given, is the skin-friction coefficient reported by the experimenters themselves. C_{flt} is the skin-friction coefficient calculated using a Ludwieg-Tillmann formula so that

$$C_{flt} = 0.246 \times 10^{-0.678H} R_\theta^{-0.268}$$ (29)

where H is the shape factor and R_θ is the Reynolds number based on momentum thickness.

The fully turbulent boundary layers are tripped at the first grid point after the leading edge and no transition-region model is used. The laminar-flow-similarity solution is used to initialize the calculations.

ID 1100

Ludwieg and Tillmann [11] studied this flow over a flat plate with a moderate adverse pressure gradient. The data downstream of 3 meters do not satisfy integral momentum balances. (See page 17 of [10] and page 66 of [12].) The reference quantities are:

11

$x(m)$	$U_e(m/s)$	$dU_e/dx(s^{-1})$
0.000	34.68	0.0
0.782	33.90	-2.30
1.282	32.60	-3.35
1.782	30.70	-4.32
2.282	28.60	-3.58
2.782	27.10	-3.00
3.132	26.05	-2.74
3.332	25.75	-2.60
3.532	24.85	-2.50
3.732	24.50	-2.40
3.932	24.05	-2.30
4.132	23.60	-2.25
4.332	23.10	-2.18

Table 1: Velocity Distribution ID 1100

$L_{ref} = 1$ m, $M_{ref} = 0.10021$, $T_{ref} = 298$ K, $P_{ref} = 1.01325 \times 10^5$ Pa.

The calculation is performed with zero heat flux at the wall. Linear interpolation is used to calculate the boundary-layer edge velocity and its streamwise gradient between the values given in Table 1.

The skin-friction coefficient as a function of streamwise distance from the leading edge is plotted in Figure 1. The three estimates of the skin-friction coefficient from the experimental data appear as discreet symbols; the triangles represent the skin-friction coefficients as determined by the experimenters, the squares indicate the skin-friction coefficients determined by the Ludwieg-Tillman formula, and the circles represent the skin-friction coefficients obtained by Coles' fit of the data to the law of the wall. The results of the three calculations are indicated by lines; the solid line shows

the results for the Cebeci-Smith model, the dashed line marks the results using the Baldwin-Lomax model, and the chain-dashed line indicates the results obtained with the TRANZ3 code. All three calculations show the same trends in the fully-turbulent regime. The Cebeci-Smith model gives the best quantitative agreement. TRANZ3 overpredicts C_f here. This is a consistent trend which will be seen in the subsequent data. Some of the jaggedness in the computed C_f curves may be attributed to the linear interpolation of the boundary-layer-edge velocities. The agreement between the computed and the experimentally determined values of C_f is acceptable within 3 meters of the leading edge. Beyond 3 meters, the discrepancies increase.

ID 1200

This flow, studied by Ludwieg and Tillmann [11], has a strong adverse pressure gradient on a flat plate. The streamwise gradient of edge velocity is approximately constant for a large portion of the flow. The data downstream of 3 meters do not satisfy momentum balances. (See page 17 of [10] and page 66 of [12].) The reference quantities are:

$L_{ref} = 1$ m, $M_{ref} = 0.08656164$, $T_{ref} = 294$ K, $P_{ref} = 1.01325 \times 10^5$ Pa.

The calculation is performed with zero heat flux at the wall. Linear interpolation is used to calculate the boundary-layer edge velocity and its streamwise gradient between the values given in Table 2.

The calculated and experimental skin-friction-coefficient distributions are illustrated in Figure 2. For $x < 3$ meters, the agreement between the experi-

$x(m)$	$U_e(m/s)$	$dU_e/dx(s^{-1})$
0.000	36.24	-4.15
0.782	33.00	-4.15
1.282	31.20	-4.15
1.782	28.80	-4.15
2.282	27.10	-4.15
2.782	24.65	-4.15
3.132	23.45	-3.80
3.332	22.90	-2.92
3.532	22.43	-1.80
3.732	22.10	-0.65
3.932	22.13	0.60

Table 2: Velocity Distribution ID 1200

mentally determined C_f and that computed using the Cebeci-Smith model is excellent. The Baldwin-Lomax model and TRANZ3 again both overpredict the skin friction coefficient. In the regions where the streamwise gradient of edge velocity is approximately constant, linear interpolation of the boundary-layer edge velocity is exact. This probably accounts for the somewhat better agreement between experiment and calculation compared with that in the previous case.

ID 1300

This flow over a flat plate with a moderate favorable pressure gradient, was also studied by Ludwieg and Tillmann [11]. The reference quantities are: $L_{ref} = 1$ m, $M_{ref} = 0.02542619$, $T_{ref} = 294$ K, $P_{ref} = 1.01325 \times 10^5$ Pa.

The calculation is performed with zero heat flux at the wall. Linear interpolation is used to calculate the boundary-layer edge velocity and its

14

$x(m)$	$U_e(m/s)$	$dU_e/dx(s^{-1})$
0.000	08.74	3.35
0.782	11.52	3.65
1.282	13.38	4.00
1.782	15.61	4.33
2.282	17.85	4.68
2.782	20.20	4.90
3.132	22.07	5.00
3.332	22.90	5.00
3.532	23.70	4.96
3.732	25.13	4.86
3.932	25.80	4.60
4.132	26.40	4.13
4.332	27.50	3.50

Table 3: Velocity Distribution ID 1300

streamwise gradient between the values given in Table 3.

In Figure 3 are plotted the skin-friction distributions as determined from the experiment and as obtained from the calculations. The Cebeci-Smith model and TRANZ3 predict skin-friction coefficients that are in excellent agreement with the experiments; the computed values are always within the range of the values obtained from the experiment. The Baldwin-Lomax model also performs well, but its values are slightly below those obtained from the experiments.

ID 1400

The experimental data for this flow over a flat plate with zero pressure gradient come from Wieghardt and Tillman [13]. The reference quantities are:

$L_{ref} = 1$ m, $M_{ref} = 0.0960$, $T_{ref} = 294$ K, $P_{ref} = 1.01325 \times 10^5$ Pa.

The calculation is performed with zero heat flux at the wall. The minor (less than 1%) variations in the free-stream velocity have almost no effect on the resulting turbulent flow and are not given here. The nominal free-stream velocity is 33.0 m/s. The skin-friction distributions are plotted in Figure 4. In this flow, all three calculations do quite well. Note that while the Cebeci-Smith and Baldwin-Lomax models give nearly identical results, TRANZ3 provides skin friction coefficients that are slightly higher than the others.

ID 3300

An ordinary turbulent boundary-layer over a flat plate is subjected to a sudden adverse pressure gradient at $x = 2$ ft. The adverse pressure gradient is then relaxed smoothly. The experiments have been performed by Bradshaw [14]. The reference quantities are:

$L_{ref} = 1$ ft, $M_{ref} = 0.1072$, $T_{ref} = 522$ R, $P_{ref} = 2.155 \times 10^3 lb_f/ft^2$.

The calculation is performed with zero heat flux at the wall. Small velocity variations in the region of nominally zero pressure gradient ($x < 2$ ft) have been smoothed. Linear interpolation is used to calculate the boundary-layer-edge velocity between the values given in Table 4. Less extensive data are available for calculating the streamwise gradient of the boundary-layer-edge velocity. Linear interpolation is used to calculate its value between the values given in Table 5. Note that the data are given (and the calculations

16

$x(ft)$	$U_e(ft/s)$		$x(ft)$	U_e
0.0	127.92		4.12500	106.44
0.375000	127.92		4.37500	104.88
1.12500	127.80		4.62500	103.32
1.62500	127.80		4.87500	102.12
1.87500	126.96		5.12500	100.56
2.12500	124.32		5.37500	99.24
2.37500	121.56		5.87500	97.20
2.62500	119.28		6.37500	95.52
2.87500	116.16		6.62500	94.20
3.12500	113.64		6.87500	93.24
3.37500	111.84		7.12500	92.52
3.62500	109.56		7.37500	91.56
3.87500	107.88		7.62500	91.20

Table 4: Velocity Distribution ID 3300

were performed) using U.S. Customary Units.

The skin-friction-coefficient distributions are shown in Figure 5. All three models give values of C_f which are greater than the experimental values. The Cebeci-Smith model gives results that are closest to the experimental values, though even here, the model's predictions are as much as 20% high.

Supersonic Case

To assess the turbulent results for supersonic flow, a comparison of the current code with the boundary-layer code of Anderson and Lewis [15] has been performed for a five degree half-angle cone at zero angle of attack with adiabatic wall boundary conditions. The edge Mach number is 1.46. The skin-friction coefficients and recovery factors computed by the two codes match to within 1% at all stations. The calculations end with $Re_x = 65 \times 10^6$.

$x(ft)$	$dU_e/dx(s^{-1})$
0.0	0.0
2.0	-11.40
2.5	-11.00
3.0	-9.30
3.5	-7.50
4.0	-6.38
5.0	-5.00
6.0	-4.19
7.0	-3.68

Table 5: Velocity-Gradient Distribution ID 3300

From these tests we have concluded that the boundary-layer code is working correctly for turbulent flows. In addition, the version of the Cebeci-Smith model used here always gives as good or better agreement with the experimental data than does our version of the Baldwin-Lomax model, hence in the transitional-flow cases discussed below, the Cebeci-Smith model is used.

3.2 Transitional-Flow Cases

Seven different types of transitional flows are studied. In most of the flows, multiple cases are investigated. In Table 6 we identify some distinctive characteristics of each of the cases and the corresponding figure number. In the appendix we give detailed instructions for obtaining the experimental data used in the figures.

In addition to the parameters required above for the fully turbulent flow cases, the transitional flows require the free-stream-turbulence level, q, and the point x_t, where the transition model is started. In theory, this position

Flow	Description	Case	Description	Figure
1	incompressible, 2D, zero pressure-gradient flow		only one case	6
2	incompressible, 2D, favorable pressure-gradient flow	1	mild acceleration	7a
		2	strong acceleration	7b
3	supersonic flow on a cone	1	$M_{ref} = 1.16$	8a
		2	$M_{ref} = 1.30$	8b
		3	$M_{ref} = 1.55$	8c
		4	$M_{ref} = 1.86$	8d
		5	$M_{ref} = 3.36$, $P_{ref} = 2.23 \times 10^4$ Pa	8e
		6	$M_{ref} = 3.36$, $P_{ref} = 1.69 \times 10^4$ Pa	8f
		7	$M_{ref} = 3.36$, $P_{ref} = 1.10 \times 10^4$ Pa	8g
4	incompressible, 2D, zero pressure-gradient flow with free-stream turbulence	1	q = 0.042 %	9a
		2	q = 0.10 %	9b
		3	q = 0.20 %	9c
		4	q = 0.26 %	9d
		5	q = 0.34 %	9e
		6	q = 0.25 %	9f
		7	q = 1.0 %	9g
		8	q = 2.0 %	9h
5	incompressible flow on a spheroid with and without roughness	1	$U_\infty = 20$ m/s, no roughness	10a
		2	$U_\infty = 20$ m/s, with roughness	10a
		3	$U_\infty = 30$ m/s, no roughness	10b
		4	$U_\infty = 30$ m/s, with roughness	10b
6	incompressible flow on a concave surface		only one case	11
7	incompressible flow on a spheroid at angle-of-attack	1	2.5 deg.	12a
		2	5.0 deg.	12b

Table 6: Transitional Flows

is where the intermittency first becomes nonzero; however, this is difficult to determine in practice. In cases where the intermittency is given, the point x_t is determined as the zero intercept of the function $F = \sqrt{-\log{(1 - \gamma(x))}}$ [5]. In cases where the intermittency is not given, but the minimum of some measured surface quantity is, we take $x_t = x_{min}/1.1$ as suggested in [5]. As far as we can determine, the proponents of the ONERA/CERT model give no recommendations as to the starting location to be used. Unless otherwise noted, the laminar-flow-similarity solution for either a cone or a flat plate (depending on the geometry) is used to initialize the calculations.

Flow 1

Schubauer and Klebanoff [16] studied the transitional flow over a flat plate in a very quiet wind tunnel. The reference quantities which we used for computing their flow are as follows:

$L_{ref} = 1$ m, $M_{ref} = 0.071$, $T_{ref} = 293$ K, $P_{ref} = 1.01325 \times 10^5$ Pa, $q = 0.03\%$, $x_t = 1.6$ m.

The calculation is performed with zero heat flux at the wall. The skin-friction coefficients are determined from velocity-profile data and are reported in [5].

Figure 6 shows the predicted and experimental skin-friction coefficients as a function of Re_x. Both the ONERA/CERT model and Narasimha's model give reasonable fits to the available data. The ONERA/CERT model tends to overpredict the skin friction maximum while Narasimha's model

20

slightly underpredicts this maximum. Results from a recent version of Dey and Narasimha's code, TRANZ3, [5] are also included in Figure 6. The sharp rise in C_f that occurs with Narasimha's model in our boundary-layer code appears with this code as well and shows up again in several of our later cases. TRANZ3 underpredicts the skin friction in the laminar boundary layer while our boundary-layer code agrees with the Blasius solution to within 1/2%. The discrepancy in the fully turbulent region is due to the turbulence modeling and is discussed above.

Flow 2

Blair and Werle [17] have studied transitional flows in favorable pressure gradients, where they made extensive heat-transfer measurements. Blair (personal communication) has provided tabulated values of local wall heat flux and Stanton number. The Stanton number is defined as:

$$St = \frac{q_w}{\rho_e c_p U_e (T_{aw} - T_e)}, \tag{30}$$

where q_w is the heat flux, T_{aw} is the adiabatic wall temperature (which for this low speed flow is the wall temperature), and T_e is the temperature at the edge of the boundary layer. The boundary-layer-edge velocity distribution is well represented by analytic expressions. The acceleration starts 0.1016 meters upstream of the leading edge of the plate. There is an unheated length of 0.043 meters at the leading edge. The reference conditions that we use for the two cases computed are based on conditions just upstream of the acceleration. Our streamwise coordinate is measured from the leading edge

21

of the plate.

Case 1: Here the flow is subjected to a mild pressure gradient. The stream-wise boundary-layer-edge velocity in meters/second is given by:

$$U_e(x) = 4.511 \times 10^3 \, (200 - x/0.0254)^{-1.066} \qquad (31)$$

where x is in meters. The reference parameters are as follows:

$L_{ref} = 1$ m, $M_{ref} = 0.04530$, $T_{ref} = 294$ K, $P_{ref} = 1.01325 \times 10^5$ Pa, $q = 2.0\%$, $x_t = 0.2122$ m.

The wall heat flux is given in Table 7. The calculated and experimental Stanton number distributions appear in Figure 7(a). Note that the different transitional-flow models give different values of the Stanton number long after both models agree that the flow is fully turbulent. This is due to the different origins of the turbulent boundary layers in the two models. The discrepancies in the laminar region are probably due to buffeting of the boundary layer in the high free-stream-turbulence environment.

Case 2: Here the flow is subjected to a strong favorable pressure gradient. The streamwise boundary-layer edge velocity in meters/second is given by:

$$U_e(x) = 1.152 \times 10^3 \, (83.3 - x/0.0254)^{-1.075} \qquad (32)$$

where x is in meters. The reference parameters are as follows:

$L_{ref} = 1$ m, $M_{ref} = 0.02746$, $T_{ref} = 294$ K, $P_{ref} = 1.01325 \times 10^5$ Pa, $q = 2.0\%$, $x_t = 0.5817$ m.

$x(m)$	$q_w(W/m^2)$	$x(m)$	$q_w(W/m^2)$
0.0556	0.5541728×10^3	0.5382	0.5325964×10^3
0.0683	0.5428168×10^3	0.5890	0.5337320×10^3
0.0810	0.5360032×10^3	0.6398	0.5337320×10^3
0.0937	0.5303252×10^3	0.6906	0.5348676×10^3
0.1064	0.5257828×10^3	0.7414	0.5348676×10^3
0.1191	0.5212404×10^3	0.7922	0.5348676×10^3
0.1318	0.5178336×10^3	0.8430	0.5348676×10^3
0.1445	0.5144268×10^3	0.8938	0.5348676×10^3
0.1572	0.5110200×10^3	0.9446	0.5337320×10^3
0.1699	0.5087488×10^3	0.9954	0.5337320×10^3
0.2007	0.5064776×10^3	1.0462	0.5337320×10^3
0.2080	0.4996640×10^3	1.0970	0.5337320×10^3
0.2334	0.5019352×10^3	1.1732	0.5337320×10^3
0.2588	0.5007996×10^3	1.2494	0.5337320×10^3
0.2842	0.5030708×10^3	1.3256	0.5337320×10^3
0.3350	0.5064776×10^3	1.4018	0.5337320×10^3
0.3858	0.5155624×10^3	1.4780	0.5348676×10^3
0.4366	0.5246472×10^3	1.5542	0.5348676×10^3
0.4874	0.5280540×10^3		

Table 7: Heat Flux Distribution for Flow 2, Case 1

$x(m)$	$q_w(W/m^2)$	$x(m)$	$q_w(W/m^2)$
0.0556	0.5484948×10^3	0.5382	0.4621892×10^3
0.0683	0.5360032×10^3	0.5890	0.4633248×10^3
0.0810	0.5280540×10^3	0.6398	0.4655960×10^3
0.0937	0.5201048×10^3	0.6906	0.4701384×10^3
0.1064	0.5144268×10^3	0.7414	0.4769520×10^3
0.1191	0.5098844×10^3	0.7922	0.4814944×10^3
0.1318	0.5042064×10^3	0.8430	0.4883080×10^3
0.1445	0.5019352×10^3	0.8938	0.4939860×10^3
0.1572	0.4962572×10^3	0.9446	0.5007996×10^3
0.1699	0.4939860×10^3	0.9954	0.5087488×10^3
0.2007	0.4905792×10^3	1.0462	0.5189692×10^3
0.2080	0.4837656×10^3	1.0970	0.5223760×10^3
0.2334	0.4814944×10^3	1.1732	0.5280540×10^3
0.2588	0.4780876×10^3	1.2494	0.5303252×10^3
0.2842	0.4758164×10^3	1.3256	0.5337320×10^3
0.3350	0.4701384×10^3	1.4018	0.5382744×10^3
0.3858	0.4655960×10^3	1.4780	0.5416812×10^3
0.4366	0.4633248×10^3	1.5542	0.5450880×10^3

Table 8: Heat Flux Distribution for Flow 2, Case 2

The wall heat flux is given in Table 8. The calculated and experimental Stanton number distributions appear in Figure 7(b). The strong favorable pressure gradient starts thinning the laminar boundary layer just before the turbulence models are initiated. This has the dramatic effect of inhibiting transition from occurring with the ONERA/CERT model.

Flow 3

The experiments we considered here were for supersonic flows over 5 degree half-angle sharp cones at zero angle of attack. In the experiments, some care was taken to eliminate any wall heat flux. The Mach numbers

24

reported here are the boundary-layer-edge Mach numbers. In all cases we use a Prandtl number of 0.71. The x coordinate is along the surface of the cone.

The first four cases have Mach numbers from 1.16 to 1.86. These are from the flight tests of Fisher and Dougherty [18]. Only the beginning and end of transition, as determined by the minimum and maximum reading from a surface pitot tube, are reported. To compare our calculations with this data, we plot the skin-friction coefficient versus Re_x, where x is the distance along the surface of the cone. The locations of the experimentally determined beginning and end of transition are indicated by vertical arrows on the top and bottom of the plot. If the models work well, the local minimum and maximum in the skin-friction coefficient should occur near the locations indicated by the arrows. The specific cases chosen have been examined by Malik [19] to assess the usefulness of e^N methods for predicting the beginning of transition. The boundary-layer-edge conditions reported by Malik are used here.

The last three cases for supersonic flows are taken from experiments performed in the Mach 3.5 Low-Disturbance Wind Tunnel at NASA Langley Research Center [20]. All three cases have the same Mach number, but they have different stagnation pressures and hence different unit Reynolds numbers. The quantity of interest reported in [20] is the distribution of recovery

factor. The recovery factor is defined as:

$$r = \frac{T_{aw} - T_e}{T_0 - T_e} \qquad (33)$$

where T_{aw} is the adiabatic wall temperature, T_0 is the stagnation temperature, and T_e is the edge temperature. The experimental recovery factors which we plot have been obtained by digitizing the data from Figure 3 of [20]. We note here that the recovery factors obtained in this experiment in the turbulent region are lower than what is typically obtained in similar flows (see Figure 23.5 of Schlichting [21]).

Both experiments have very low free-stream-turbulence levels; however, the low free-stream-turbulence correction in Narasimha's model is not used in these supersonic flows since the correction is calibrated only from incompressible flow data and is not intended to be used simultaneously with the high Mach number correction.

Case 1: This case is from Flight 333 at time 13:43. The reference quantities are:

$L_{ref} = 1$ m, $M_{ref} = 1.16$, $T_{ref} = 229.0$ K, $P_{ref} = 2.5469 \times 10^4$ Pa, $q = 0.1\%$, $x_t = 0.6964$ m.

The skin-friction coefficient as a function of Re_x is plotted in Figure 8(a). In the experiments, the minimum surface pitot-tube pressure (beginning of transition) occurs at $Re_x = 7.02 \times 10^6$ and the local maximum surface pitot-tube pressure (end of transition) occurs at $Re_x = 7.71 \times 10^6$. The ON-ERA/CERT model appears to do somewhat better than Narasimha's model

26

here.

Case 2: This case is from Flight 330 at time 9:39. The reference quantities are:

$L_{ref} = 1$ m, $M_{ref} = 1.30$, $T_{ref} = 221.6$ K, $P_{ref} = 2.2034 \times 10^4$ Pa, $q = 0.1\%$, $x_t = 0.5497$ m.

The skin-friction coefficient as a function of Re_x is plotted in Figure 8(b). In the experiments, the minimum surface pitot-tube pressure (beginning of transition) occurs at $Re_x = 5.61 \times 10^6$ and the local maximum surface pitot-tube pressure (end of transition) occurs at $Re_x = 6.58 \times 10^6$. The ON-ERA/CERT model appears to do somewhat better than Narasimha's model here.

Case 3: This case is from Flight 339 at time 13:08. The reference quantities are:

$L_{ref} = 1$ m, $M_{ref} = 1.55$, $T_{ref} = 223.8$ K, $P_{ref} = 2.3310 \times 10^4$ Pa, $q = 0.1\%$, $x_t = 0.6210$ m.

The skin-friction coefficient as a function of Re_x is plotted in Figure 8(c). In the experiments, the minimum surface pitot-tube pressure (beginning of transition) occurs at $Re_x = 7.89 \times 10^6$ and the local maximum surface pitot-tube pressure (end of transition) occurs at $Re_x = 9.13 \times 10^6$. The ON-ERA/CERT model appears to do somewhat better than Narasimha's model here.

Case 4: This case is from Flight 343 at time 12:32. The reference quantities

27

are:

$L_{ref} = 1$ m, $M_{ref} = 1.86$, $T_{ref} = 222.0$ K, $P_{ref} = 2.3604 \times 10^4$ Pa, $q = 0.1\%$, $x_t = 0.4650$ m.

The skin-friction coefficient as a function of Re_x is plotted in Figure 8(d). In the experiments, the minimum surface pitot-tube pressure (beginning of transition) occurs at $Re_x = 7.29 \times 10^6$ and the local maximum surface pitot-tube pressure (end of transition) occurs at $Re_x = 8.85 \times 10^6$. Narasimha's model appears to do somewhat better than the ONERA/CERT model here.

Case 5: This case is based on the topmost case of Figure 3 in [20]. The reference quantities appear below.

$L_{ref} = 1$ m, $M_{ref} = 3.36$, $T_{ref} = 97.87$ K, $P_{ref} = 2.2287 \times 10^4$ Pa, $q = 0.1\%$, $x_t = 0.0815$ m.

The recovery factor as a function of Re_x is plotted in Figure 8(e). The continuously rising recovery factor in the turbulent regime has also been observed with another boundary-layer code using a somewhat different turbulence model [22]. The differences between the experimental results and the calculations in terms of wall temperature are less than 4 Kelvin, or about 1.2% of the stagnation temperature. It is possible that this problem might be alleviated using a turbulence model with a variable turbulent Prandtl number.

Case 6: This case is based on the third case of Figure 3 in [20]. The reference quantities are:

$L_{ref} = 1$ m, $M_{ref} = 3.36$, $T_{ref} = 98.09$ K, $P_{ref} = 1.6887 \times 10^4$ Pa, $q = 0.1\%$, $x_t = 0.1174$ m.

The recovery factor as a function of Re_x is plotted in Figure 8(f). The comments of the previous case also apply here.

Case 7: This case is based on the fifth case of Figure 3 in [20]. The reference quantities are:

$L_{ref} = 1$ m, $M_{ref} = 3.36$, $T_{ref} = 98.00$ K, $P_{ref} = 1.1022 \times 10^4$ Pa, $q = 0.1\%$, $x_t = 0.2166$ m.

The recovery factor as a function of Re_x is plotted in Figure 8(g).

Flow 4.

We considered two series of experiments that investigated the effects of free-stream turbulence on transition. The first series was done by Schubauer and Skramstad [23] on a flat plate with zero pressure gradient. The beginning and end of transition were determined by the local minimum and maximum in surface pitot-tube pressure. We chose five cases from their work, all with free-stream-turbulence levels less than 0.4%. In plots of our results, vertical arrows indicate the experimentally determined beginning and end of transition. For greater values of free-stream turbulence, we used the heat-transfer experiments of Blair [24] on a zero pressure gradient flat plate. The constant heat-flux plate used here is the same as that used in Flow 2. We considered up to 2% free-stream-turbulence levels. Tabulated Stanton number values were provided by Blair (personal communication).

29

Case 1: The wall is assumed to be adiabatic. The flow parameters are as follows:

$L_{ref} = 1$ m, $M_{ref} = 0.071$, $T_{ref} = 293$ K, $P_{ref} = 1.01325 \times 10^5$ Pa, $q = 0.042\%$, $x_t = 1.603$ m.

The skin friction as a function of Re_x is plotted in Figure 9(a). In the experiments, the minimum surface pitot-tube pressure occurs at $Re_x = 2.85 \times 10^6$ and the local maximum surface pitot-tube pressure (end of transition) occurs at $Re_x = 3.85 \times 10^6$. Here both models do reasonably well, though the ONERA/CERT model does somewhat better.

Case 2: The flow parameters that differ from Case 1 are as follows:

$q = 0.10\%$, $x_t = 1.5454$ m.

The skin friction as a function of Re_x is plotted in Figure 9(b). In the experiments, the minimum surface pitot-tube pressure occurs at $Re_x = 2.75 \times 10^6$ and the local maximum surface pitot-tube pressure occurs at $Re_x = 3.95 \times 10^6$. The experimentally determined end of transition should correspond closely with the skin-friction peak. The ONERA/CERT model has its skin-friction peak occurring too soon. This problem gets worse in later cases.

Case 3: The flow parameters that differ from Case 1 are as follows:

$q = 0.20\%$, $x_t = 1.2373$ m.

The skin friction as a function of Re_x is plotted in Figure 9(c). In the experiments, the minimum surface pitot-tube pressure occurs at $Re_x = 2.20 \times$

10^6 and the local maximum surface pitot-tube pressure occurs at $Re_x = 3.70 \times 10^6$. The skin-friction peak in the ONERA/CERT model continues to shift upstream.

Case 4: The flow parameters that differ from Case 1 are as follows:

$q = 0.26\%$, $x_t = 1.0118$ m.

The skin friction as a function of Re_x is plotted in Figure 9(d). In the experiments, the minimum surface pitot-tube pressure occurs at $Re_x = 1.80 \times 10^6$ and the local maximum surface pitot-tube pressure occurs at $Re_x = 3.20 \times 10^6$. Narasimha's model now does a much better job of predicting the transition length than does the ONERA/CERT model.

Case 5: The flow parameters that differ from Case 1 are as follows:

$q = 0.34\%$, $x_t = 0.7873$ m.

The skin friction as a function of Re_x is plotted in Figure 9(e). In the experiments, the minimum surface pitot-tube pressure occurs at $Re_x = 1.40 \times 10^6$ and the local maximum surface pitot-tube pressure occurs at $Re_x = 2.65 \times 10^6$. As before, Narasimha's model does much better than the ONERA/CERT one here.

Case 6: There is an unheated starting length of 0.043 meters. This is followed by a constant heat-flux flat plate which we assume is $540 W/m^2$. The flow parameters are as follows:

$L_{ref} = 1$ m, $M_{ref} = 0.0871$, $T_{ref} = 295$ K, $P_{ref} = 1.01325 \times 10^5$ Pa, $q = 0.25\%$, $x_t = 0.548$ m.

31

The Stanton number as a function of Re_x is plotted in Figure 9(f). The ONERA/CERT model does an excellent job of predicting the Stanton number in this case. Narasimha's model gives a much larger Stanton number peak than is observed experimentally.

Case 7: The flow parameters that differ from Case 6 are as follows: $M_{ref} = 0.0873$, $q = 1.0\%$, $x_t = 0.216$ m.

The Stanton number as a function of Re_x is plotted in Figure 9(g). The ONERA/CERT model still does a satisfactory job here. Narasimha's model, as in the previous case, overpredicts the Stanton number peak and a considerable downstream distance is required for the fully turbulent values of the Stanton number to agree with both the experiments and the ONERA/CERT model.

Case 8: The flow parameters that differ from Case 6 are as follows: $M_{ref} = 0.0870$, $q = 2.0\%$, $x_t = 0.122$ m.

The Stanton number as a function of Re_x is plotted in Figure 9(h). Again Narasimha's model overpredicts the Stanton number peak and requires a long distance downstream to match the fully turbulent values. We attribute the fairly large discrepancies in what ought to be the laminar flow to the buffeting of the laminar boundary layer by free-stream turbulence.

Flow 5.

In this flow we studied the effects of a roughness strip on the transition of a boundary layer over a prolate spheroid at zero angle of attack. The exper-

iments were carried out by Meier, Kreplin, and Ming [25]. Much additional data were provided by Kreplin (personal communication). The spheroid had eccentricity, $e = 1/6$, and the major axis, $2a$, was 2.4 meters long. The roughness strip consisted of sandpaper grains with an average diameter of 0.0007 meters which was blown onto liquid glue on the model surface. The strip had a leading edge at $x/(2a) = 0.2$ and extended 0.02 meters downstream. The potential-flow solution around a spheroid was used for the boundary-layer-edge velocity. The stagnation-flow solution was used to initialize the flow at the nose. In Narasimha's model, a fully turbulent boundary layer was required to start at x_t. The laminar-flat-plate-flow similarity solution was used to initialize this calculation. Shear stress was measured directly using surface hot films. Here we calculated the flow for two different free-stream velocities. For both velocities, one case was without the roughness, a second case was with the roughness. Note that the skin-friction coefficient reported here was normalized with the free-stream, not the local edge velocity.

Case 1: This case does not have a roughness strip. The reference quantities are as follows:

$L_{ref} = 2.4$ m, $M_{ref} = 0.05828$, $T_{ref} = 293$ K, $P_{ref} = 1.01325 \times 10^5$ Pa, $q = 0.2\%$, $x_t/(2a) = 0.6680$.

Case 2: This case does have a roughness strip. All of the reference quantities except for x_t are the same as in Case 1. In this case $x_t/(2a) = 0.2802$.

Figure 10(a) illustrates the skin friction coefficient based on free-stream

quantities as a function of axial distance for Cases 1 and 2. In both cases the ONERA/CERT model overpredicts the skin-friction peak. Narasimha's model underpredicts the peak for the case in which the roughness strip is included.

Case 3: This case does not have a roughness strip. The reference quantities are as follows:

L_{ref} = 2.4 m, M_{ref} = 0.08742, T_{ref} = 293 K, P_{ref} = 1.01325 × 10^5 Pa, q = 0.2%, $x_t/(2a)$ = 0.5123 .

Case 4: This case does have a roughness strip. All of the reference quantities except for x_t are the same as in Case 3. In this case $x_t/(2a)$ = 0.2037.

Figure 10(b) illustrates the skin friction coefficient based on free-stream quantities as a function of axial distance for Cases 3 and 4. Neither model correctly predicts the relatively gradual rise in skin friction for the case without the roughness strip. Narasimha's model might have performed much better had the model been initiated further downstream. The ONERA/CERT model does a very poor job in this case. The adverse pressure gradient on the back side of the spheroid causes the momentum thickness to grow quickly. This triggers an overly rapid transition with the ONERA/CERT model.

Flow 6.

The effects of streamwise curvature were studied here. The experiment was done by Swearingen and Blackwelder [26] on the concave surface of a curved plate with a 3.2 meter radius of curvature. Additional data were

34

supplied by Swearingen (private communication). For this work we assumed that the boundary-layer-edge velocity was constant. Because of the presence of strong Görtler vortices in this flow, the shear stress had large spanwise variations. At each streamwise location, the maximum and minimum shear stresses were determined from measurements of the streamwise-velocity profiles at multiple spanwise locations. The position of the minimum shear stress in the high-speed region was used to determine x_t.

The reference quantities are as follows:

$L_{ref} = 1.0$ m, $M_{ref} = 0.01457$, $T_{ref} = 293$ K, $P_{ref} = 1.01325 \times 10^5$ Pa, $q = 0.07\%$, $x_t = 0.545$ m.

The experimentally determined maximum (in the high speed region) and minimum (in the low speed region) skin-friction coefficients are plotted in Figure 11 along with the results of the two models. The models seem to do a satisfactory job of predicting the shear stress in the high-speed region. The discrepancy between models and experiment in the fully turbulent regime are probably due to experimental difficulties in determining the shear stress from low-resolution velocity profiles.

Flow 7.

Three-dimensional boundary layers were studied here. The experiments of Meier and Kreplin [27] on a smooth prolate spheroid at nonzero angle of attack were used. Except for the absence of a roughness strip, the spheroid model was the same as that used in Flow 5. Extensive tabulated data were

35

provided by Kreplin (personal communication). Some of these data were included in a DFVLR data report [28]. Only two angles of attack, 2.5 degrees and 5 degrees, had boundary layers that remained attached at all measurement stations. The potential-flow solutions were used to obtain the boundary-layer-edge velocities. The x direction was taken along the major axis of the spheroid. The calculations used 6 degree intervals in the azimuthal direction. The stagnation-flow solution was used at the first axial gridpoint. This point, $x/(2a) = 0.0004$, was taken slightly downstream of the actual stagnation point, so there was no reversed flow. A new three-tier wall-normal grid stretching technique was used in computing this flow. The standard exponential stretching was used in the lower portion of the boundary layer; the grid size was then increased linearly in the next tier; and finally the grid size was kept constant in the upper level. This multiple-level grid helped to eliminate some of the numerical problems associated with the large azimuthal variations of the boundary-layer thickness.

For the 2.5 degree angle-of-attack case, the location of the minimum skin friction and hence the point $x_t = x_{min}/1.1$, was independent of azimuthal location. For the 5 degree angle-of-attack case, the skin friction minimum varied in the azimuthal direction. Because there were a large number of hot film probes in the azimuthal direction, but not in the axial direction, our usual approach for determining x_t resulted in large axial distances between x_t locations at points which were separated by only 6 degrees in the azimuthal

36

direction. To smooth such sharp discontinuities, we used linear interpolation over several spanwise points to shift the x_t locations. The values of x_t that we used are given in the description of each case.

Case 1: This case has an angle of attack of 2.5 degrees. The reference quantities are as follows:

$L_{ref} = 2.4$ m, $M_{ref} = 0.131$, $T_{ref} = 293$ K, $P_{ref} = 1.01325 \times 10^5$ Pa, $q = 0.2\%$, $x_t/(2a) = 0.359$ at all azimuthal stations.

The total-skin-friction coefficient normalized on free-stream (not boundary-layer-edge) quantities is shown as a function of axial distance along the spheroid in Figure 12(a). The results of both Narasimha's model and the ONERA/CERT model are shown. The ONERA/CERT model produces its characteristic overshoot at all spanwise locations.

Case 2: This case has an angle of attack of 5.0 degrees. As discussed above, the values of $x_t/(2a)$ used at the various azimuthal stations are given in Table 9.

In this case, the laminar flow over the spheroid would have separated at an axial location that was still in the transition region. Because of this, Narasimha's model cannot be used since it requires a mixing of the laminar flow that would have existed and a turbulent flow originating at x_t. In addition to the separation problem, the variation of x_t in the azimuthal direction makes the initiation of the turbulent boundary layer difficult to implement. To be done correctly, the grid used to calculate the turbulent

Angle (deg)	$x_t/(2a)$		Angle (deg)	$x_t/(2a)$
0 (windward side)	0.436		96	0.281
6	0.421		102	0.281
12	0.405		108	0.281
18	0.390		114	0.320
24	0.374		120	0.359
30	0.359		126	0.333
36	0.359		132	0.307
42	0.359		138	0.281
48	0.359		144	0.281
54	0.333		150	0.281
60	0.307		156	0.281
66	0.281		162	0.281
72	0.281		168	0.281
78	0.281		174	0.281
84	0.281		180	0.281
90	0.281			

Table 9: x_t Distribution for Flow 7, Case 2

boundary layer must be designed so that the domain of dependence of the differencing scheme is restricted to the turbulent region of the flow. A different grid must be used for different distributions of x_t. The results obtained using the ONERA/CERT model are plotted in Figure 12(b). As in Case 1, the total-skin-friction coefficients are normalized on free-stream quantities. In the far downstream region $(x/(2a) \geq 0.8)$, with azimuthal angles around 144 degrees, the calculated skin-friction coefficient suddenly rises. In this region, there is strong crossflow near the wall towards the **windward** symmetry line. One can think of this as a crossflow-boundary-layer separation. The differencing scheme in the boundary-layer code is not designed to handle this type of crossflow. Since the problem occurs relatively far downstream, results pertaining to the transition region are not affected.

4 Summary

In this report, both the Baldwin-Lomax and Cebeci-Smith turbulence models were used to compute five two-dimensional, attached boundary-layer test flows with varying types of pressure gradients and one supersonic boundary layer on a cone. In all cases, the Cebeci-Smith model produced results which were as good or better than those produced by the Baldwin-Lomax model. The Cebeci-Smith model was then used to generate the turbulent flow field used with Narasimha's transition-region model. The Cebeci-Smith model was also used to calculate μ_t for the ONERA/CERT transition-region model.

Seven different kinds of transitional flow were studied, each having several cases. The extensive testing helped us to identify a few serious problems.

1. The ONERA/CERT model failed to predict any transition for the strong favorable pressure-gradient case (Flow 2, Case 2).

2. Narasimha's model could not be used for the case of a prolate spheroid with an angle of attack of 5.0 degrees (Flow 7 Case 2) because the laminar flow would have separated.

3. When using Narasimha's model, a turbulent boundary layer that started with zero thickness at x_t was required. This would have been difficult to do for the case of a prolate spheroid with an angle of attack of 5.0 degrees (Flow 7 Case 2) because x_t varies with the spanwise coordinate.

Some other issues that we found to be important in determining the accuracy of the models are summarized below. The transitional flow results depend strongly on the fully turbulent flow model. Deficiencies in a turbulence model that is incorporated into a transition-region model will be noticed in the transitional-flow region. More reasonable methods for initiating the transitional-flow model need to be developed. In our results, there are several cases where the agreement could have been improved if x_t were chosen differently. For Narasimha's model, a correlation to determine x_{t2} must also be developed. In the heat-transfer experiments, Narasimha's model consistently overpredicts the maximum Stanton number. Separate intermittency

parameters may be needed for the momentum and thermal boundary layers.

It is hoped that this report will form the basis for extensive testing of transition-region models in the future.

Acknowledgements

Appendix. Obtaining Data Used in Figures

To facilitate future comparisons with a wide range of experimental data, the distributions of experimentally determined mean-flow quantities that we used for comparison are available in the form of ASCII files. For those with NAS accounts, the files are globally readable on the NAS mass storage system in directory "/u/ps/singer/portland91". Each case for each flow has a separate subdirectory. The data for each case is in a file called "data". The flow and case identification numbers are the same as those used here. For example: "/u/ps/singer/portland91/flow2/case1/data" contains the experimental data associated with Flow 2, Case 1, a mild favorable pressure gradient case.

For those who would like the data, but do not have NAS accounts, the UNIX "tar" command has been used to put the entire directory structure

41

described above into a single file. This file will be sent via electronic mail to those who request it. Send requests to:

singer@cmb00.larc.nasa.gov

References

[1] Baldwin, B. S. and Lomax, H. 1978: Thin Layer Approximation and Algebraic Model for Separated Turbulent Flows, *AIAA Paper No. 78-257.*

[2] Cebeci, T. and Smith, A. M. O. 1974: "Analysis of Turbulent Boundary Layers," *Applied Mathematics and Mechanics,* Vol. **15**, Academic Press, New York.

[3] Bradshaw, P., Cebeci, T., and Whitelaw, J. H. 1981: *Engineering Calculation Methods for Turbulent Flow,* Academic Press, New York, pp. 43–44.

[4] Harris, J. E. and Blanchard, D. K. 1982: Computer Program for Solving Laminar, Transitional, or Turbulent Compressible Boundary-Layer Equations for Two-Dimensional and Axisymmetric Flow, *NASA TM 83207.*

[5] Dey, J. and Narasimha, R. 1988: An Integral Method for the Calculation of 2D Transitional Boundary Layers, *Report 88 FM 7,* Department of Aerospace Engineering, Indian Institute of Science, Bangalore, India.

[6] Narasimha, R. 1985: The Laminar-Turbulent Transition Zone in the Boundary Layer, *Prog. Aerospace Sci.,* Vol. **22**, pp. 29–80.

[7] Arnal, D. 1986: Three-Dimensional Boundary Layers: Laminar-Turbulent Transition, AGARD-FDP-VKI Special Course on *Calcul Des Limites Tridimensionnelles Avec Ou Sans Decollement*, 14-18 April.

[8] Arnal, D. 1988: Laminar-Turbulent Transition Problems in Supersonic and Hypersonic Flows, AGARD/FDP/VKI Special Course on *Aerothermodynamics of Hypersonic Vehicles*, 30 May – 3 June.

[9] Iyer, V. 1990: Computation of Three-Dimensional Compressible Boundary Layers to Fourth Order Accuracy on Wings and Fuselages, *NASA CR-4269*.

[10] Coles, D. E. and Hirst, E. A., editors, 1968: Vol. 2, *Proc. Comput. Turbul. Boundary-Layers*, Mechanical Engineering Department, Stanford Univ., Stanford, CA.

[11] Ludwieg, H. and Tillmann, W. 1950: Investigations of the Wall-Shearing Stress in Turbulent Boundary Layers, *NACA TM 1285*.

[12] Kline, S. J., Cockrell, D. J., Morkovin, M. V. and Sovran, G., editors, 1968: Vol. 1, *Proc. Comput. Turbul. Boundary-Layers*, Mechanical Engineering Department, Stanford Univ., Stanford, CA.

[13] Wieghardt, K. and Tillman, W. 1951: On the Turbulent Friction Layer for Rising Pressure, *NACA TM 1314*.

[14] Bradshaw, P. 1969: The Response of a Constant-Pressure Turbulent Boundary Layer to the Sudden Application of an Adverse Pressure Gradient, *R. & M. No. 3575, British Aeronautical Research Council.*

[15] Anderson, C. and Lewis, C. H. 1971: Laminar or Turbulent Boundary-Layer Flows of Perfect Gases or Reacting Gas Mixtures in Chemical Equilibrium, *NASA CR-1893.*

[16] Schubauer, G. B. and Klebanoff, P. S. 1955: Contributions on the Mechanics of Boundary-Layer Transition, *NASA TN 3489.*

[17] Blair, M. F. and Werle, M. J. 1981: Combined Influence of Free-Stream Turbulence and Favorable Pressure Gradients on Boundary Layer Transition and Heat Transfer, *United Technologies Report No. R81-914388-17.*

[18] Fisher, D. F. and Dougherty, N. S. 1982: Transition Measurements on a 10° Cone at Mach Numbers from 0.5 to 2.0, *NASA TP-1971.*

[19] Malik, M. R. 1984: Instability and Transition in Supersonic Boundary Layers, Proceedings of Energy Sources Technology Conference, New Orleans, Feb. 12–16, in *ASME Fluids Engineering Division Vol 11*, pp. 139–147.

[20] Chen, F.-J., Malik, M. R. and Beckwith, I. E. 1989: Boundary-Layer Transition on a Cone and Flat Plate at Mach 3.5, *AIAA J.*, **27**, pp. 687–693.

[21] Schlichting, H. 1979: *Boundary Layer Theory*, 7th Edition, McGraw-Hill Book Company, New York, p. 714.

[22] Singer, B. A., Dinavahi, S., and Zang, T. A. 1990: Evaluation of a Compressible Flow Transition Model, *NASP CR-1109*.

[23] Schubauer, G. B. and Skramstad, H. K. 1948: Laminar-Boundary-Layer Oscillations and Transition on a Flat Plate, *NACA Report No. 909*.

[24] Blair, M. F. 1983: Influence of Free-stream Turbulence on Boundary Layer Heat Transfer and Mean Profile Development, Part 1 – Experimental Data, *Trans. of the ASME, J. of Heat Transfer*, Vol. **105**, pp. 33–40.

[25] Meier, H. L., Kreplin and H. P, Ming, X. 1983: Problems Associated with Artificial Boundary Layer Transition, *AIAA Paper No. 83-1673*.

[26] Swearingen, J. D. and Blackwelder, R. F. 1987: The Growth and Breakdown of Streamwise Vortices in the Presence of a Wall, *J. Fluid Mech.*, Vol. **182**, pp 255–290.

[27] Meier, H. L. and Kreplin, H. P. 1980: Experimental Investigation of the Boundary Layer Transition and Separation on a Body of Revolution, *Z. Flugwiss. Weltraumforsch.*, Vol. 4, pp. 65–71.

[28] Kreplin, H. P., Vollmers, H., and Meier, H. U. 1985: Wall Shear Stress Measurements on an Inclined Prolate Spheroid in the DFVLR 3m x 3m Low Speed Wind Tunnel, Göttingen, *DFVLR Report IB 222-84 A 33.*
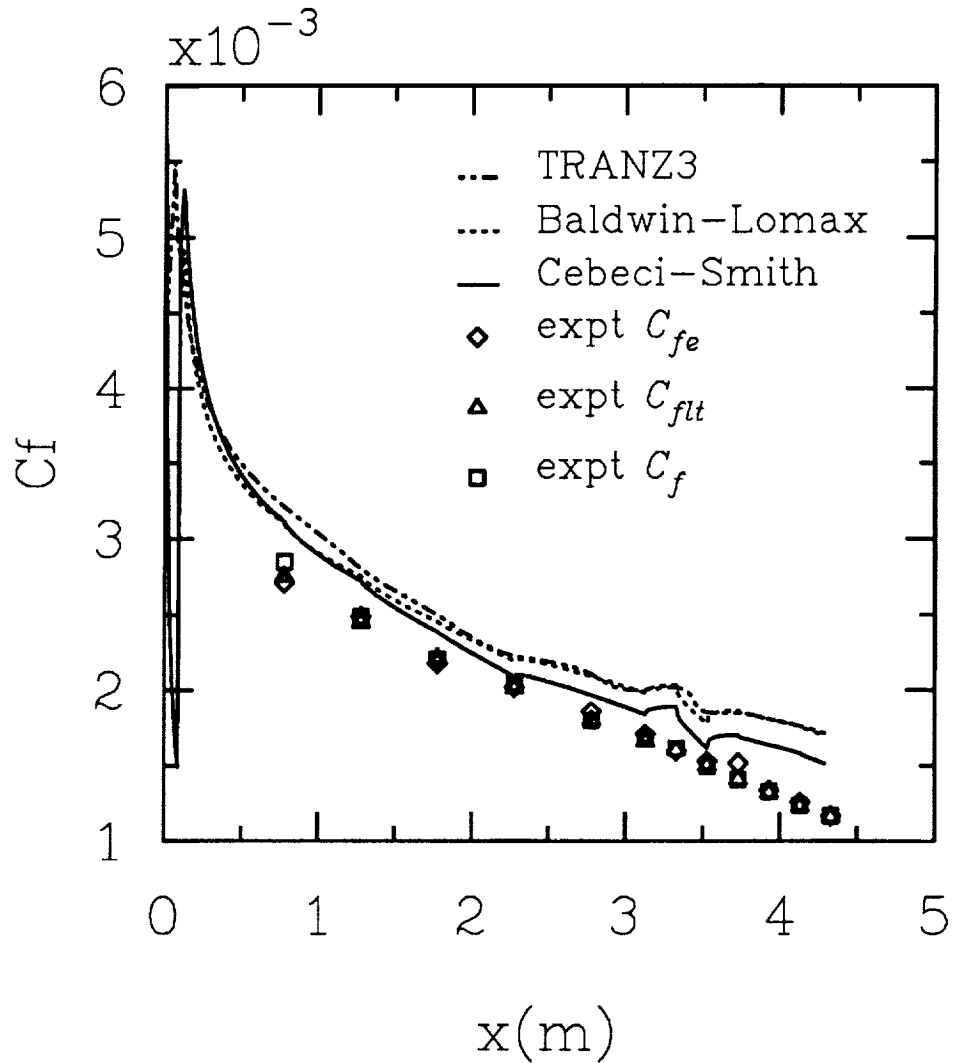
Figure 1. Fully turbulent flow with a moderately adverse pressure gradient (Flow ID 1100). Symbols correspond to different ways of determining skin friction (see [10]) from the data of Ludwieg and Tillman [11].
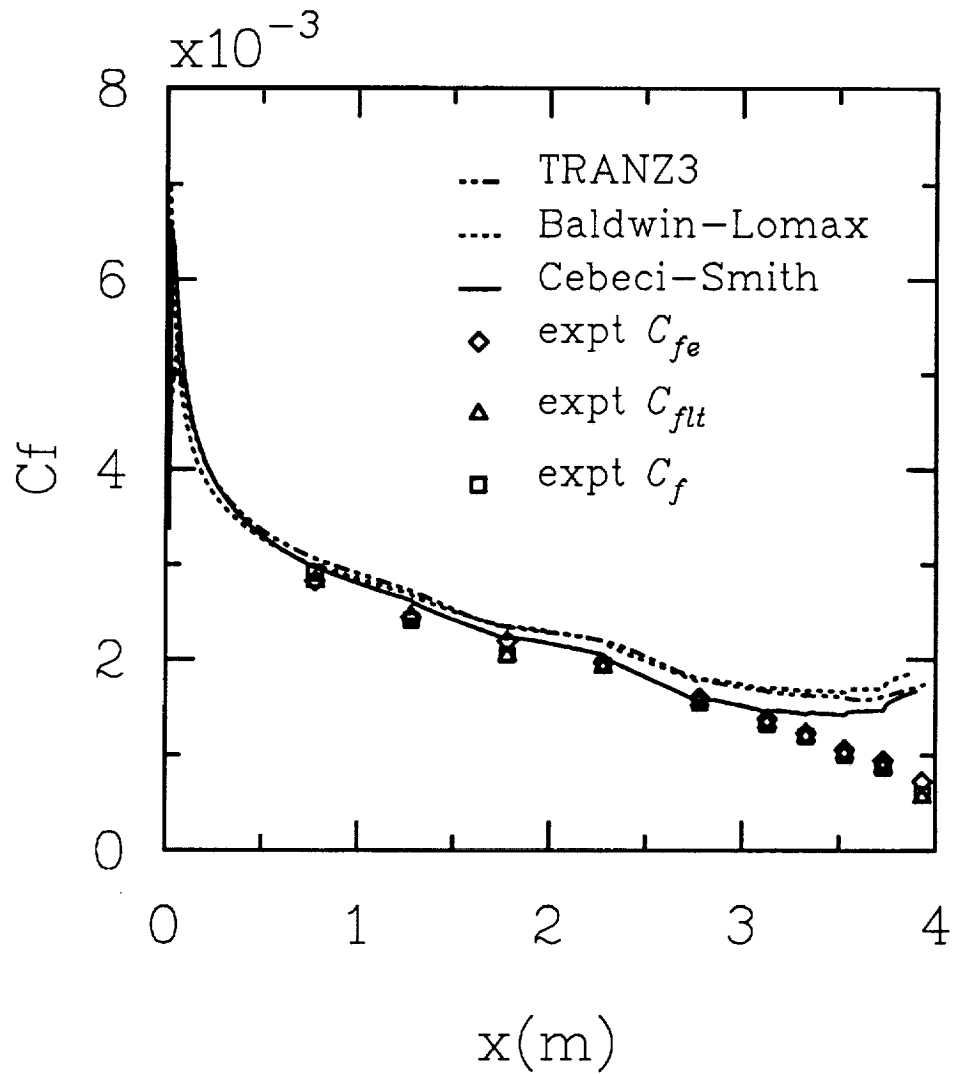
Figure 2. Fully turbulent flow with a strongly adverse pressure gradient (Flow ID 1200). Symbols correspond to different ways of determining skin friction (see [10]) from the data of Ludwieg and Tillman [11].
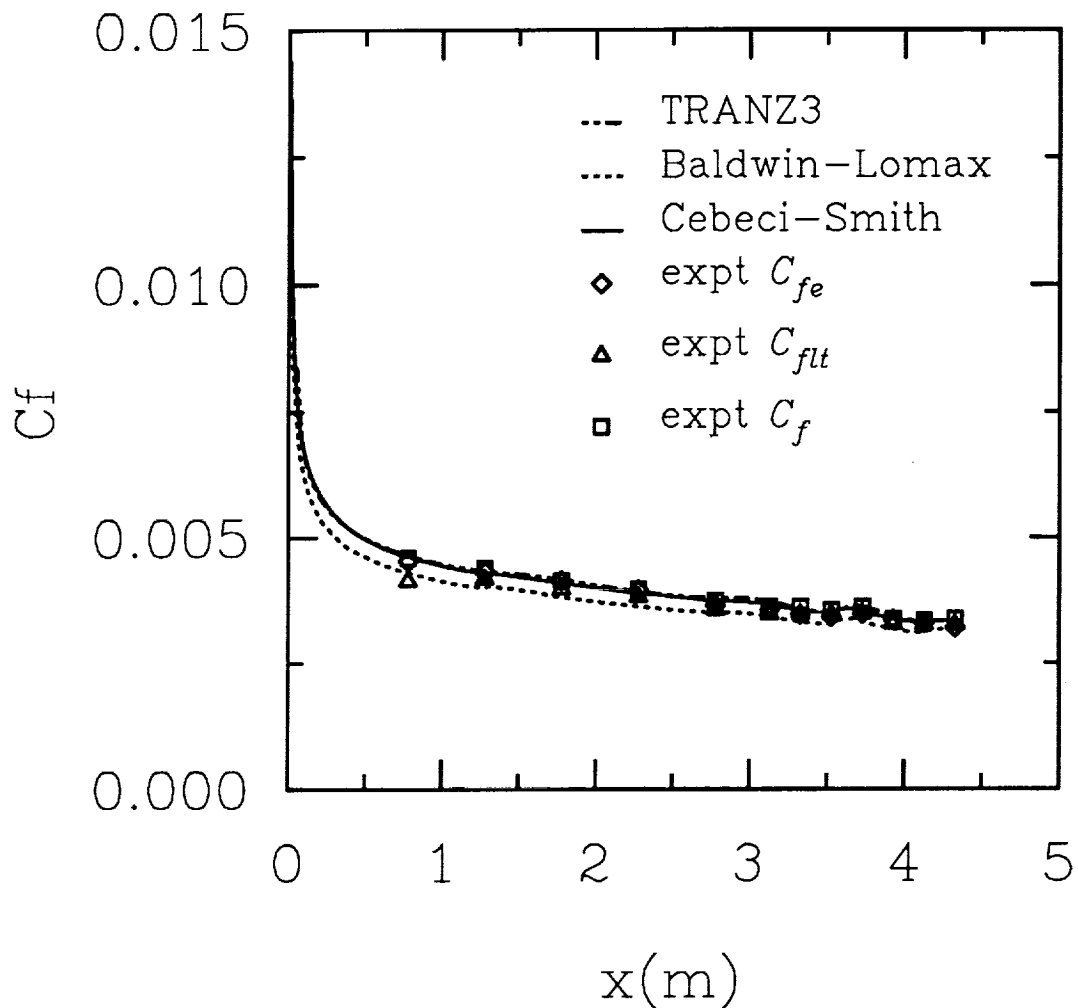
Figure 3. Fully turbulent flow with a favorable pressure gradient (Flow ID 1300). Symbols correspond to different ways of determining skin friction (see [10]) from the data of Ludwieg and Tillman [11].
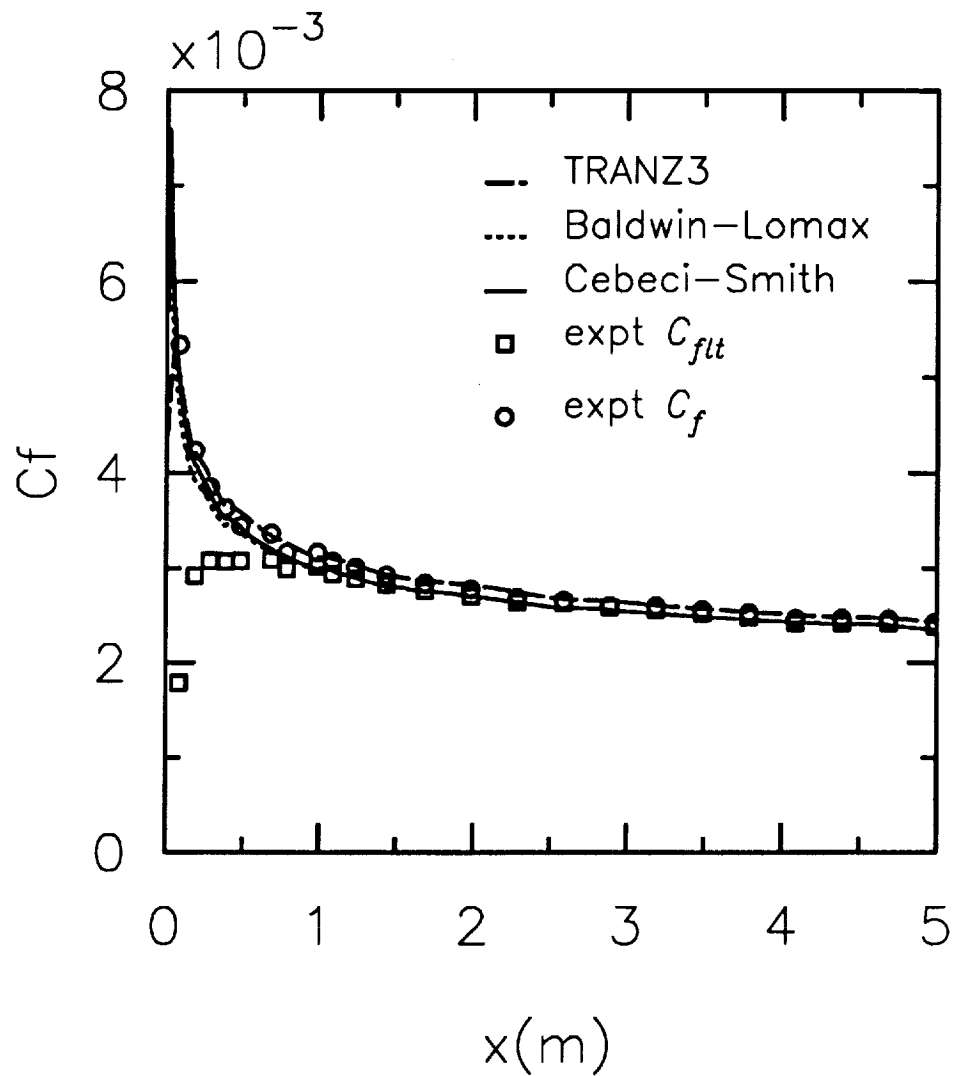
Figure 4. Fully turbulent flow with a zero pressure gradient (Flow ID 1400). Symbols correspond to different ways of determining skin friction (see [10]) from the data of Wieghardt and Tillman [13].
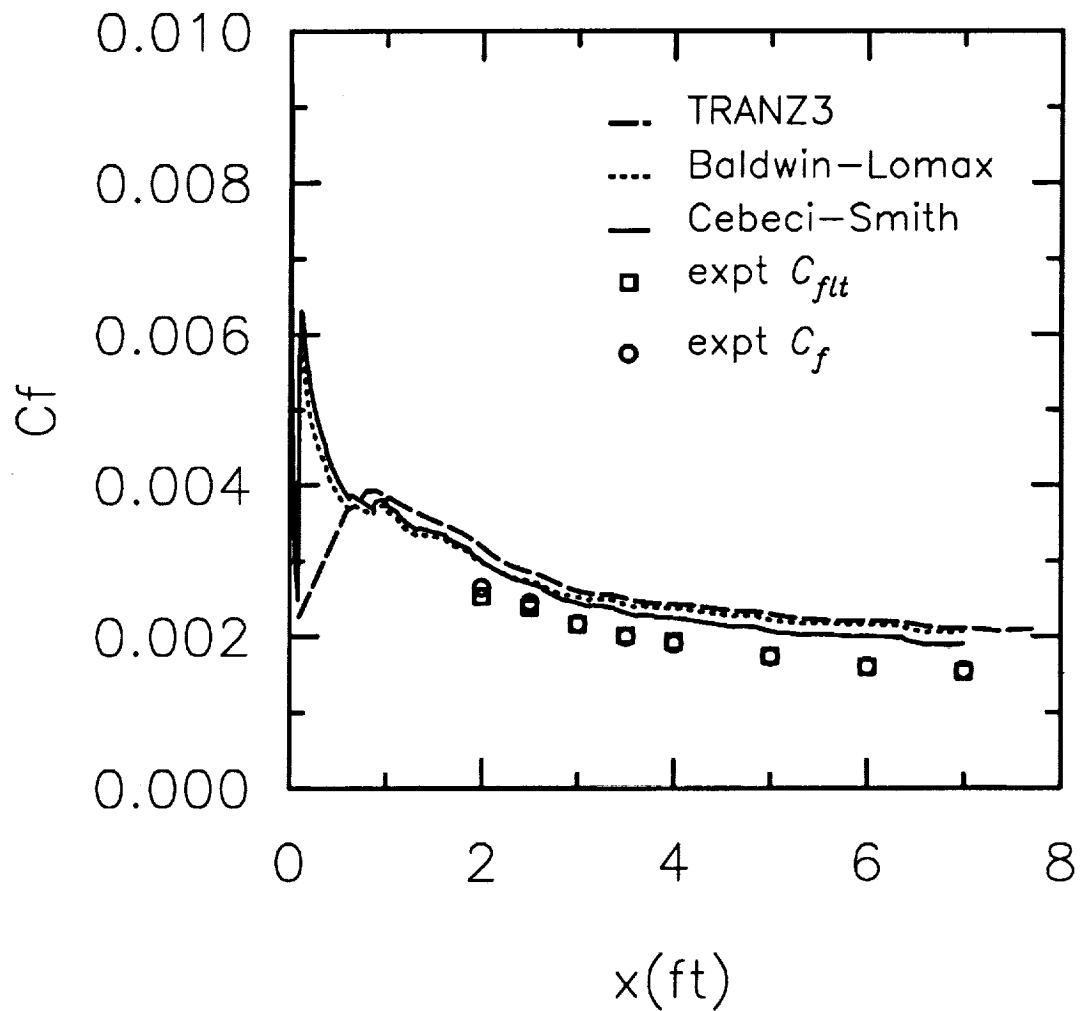
Figure 5. Fully turbulent flow with a strongly adverse pressure gradient that is gradually relaxed (Flow ID 3300). Symbols correspond to different ways of determining skin friction (see [10]) from the data of Bradshaw [14].
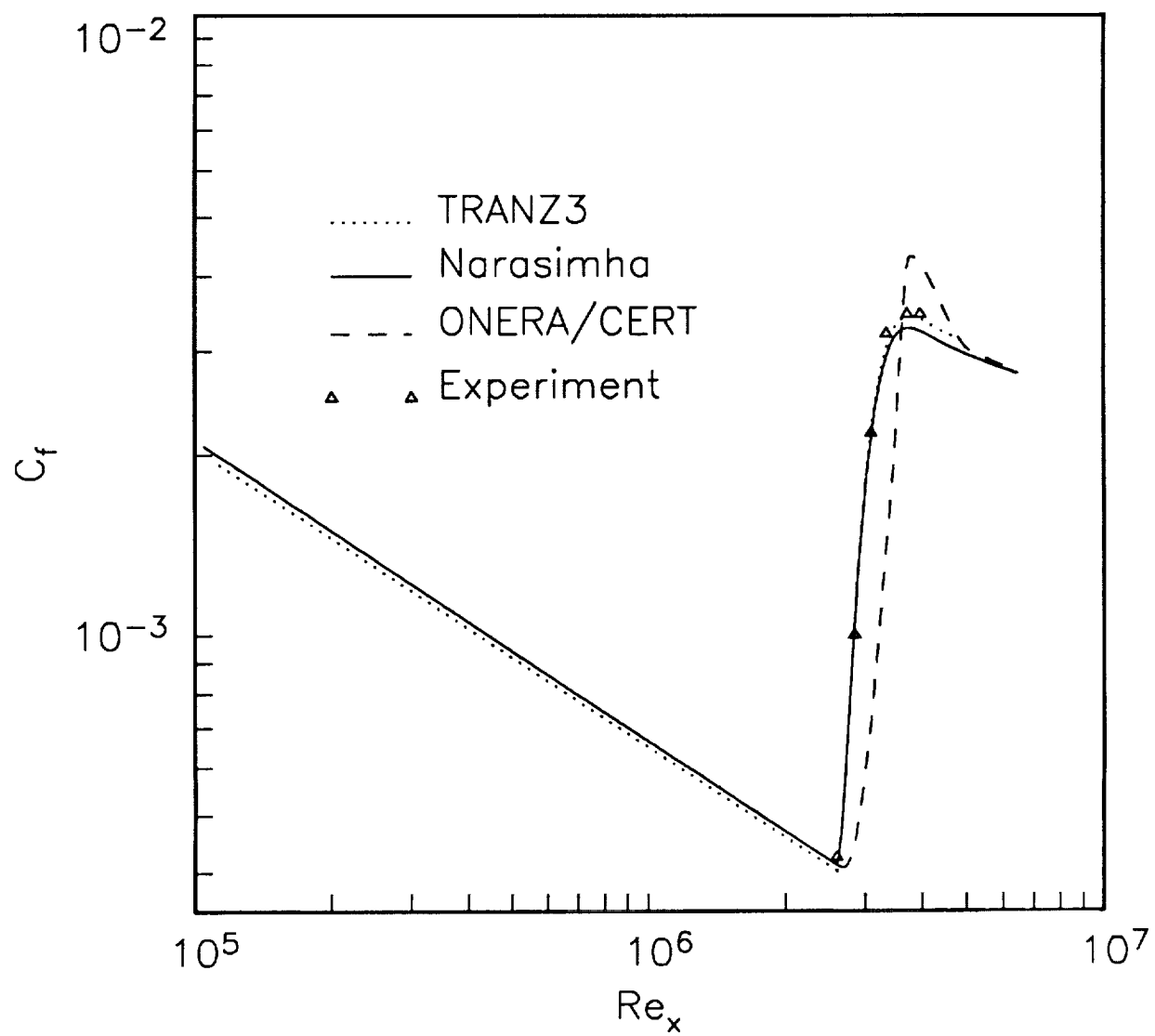
Figure 6. Transitional flow with a zero pressure gradient (Flow 1). Experiments of Schubauer and Klebanoff [16].
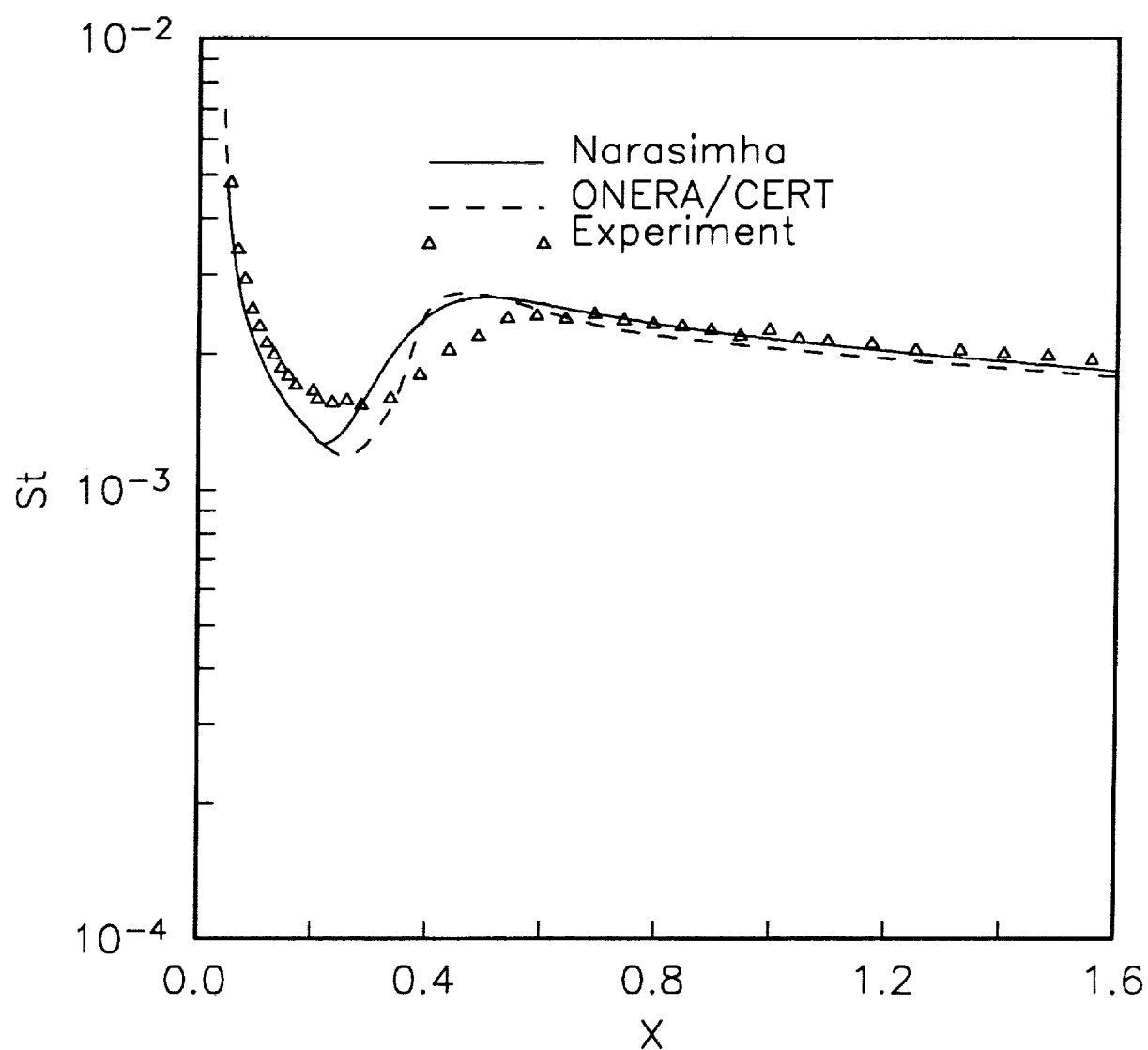
Figure 7(a). Transitional flow with a mildly favorable
pressure gradient (Flow 2, Case 1).
Experimental data from Blair and Werle [17]
and Blair (personal communication).

54
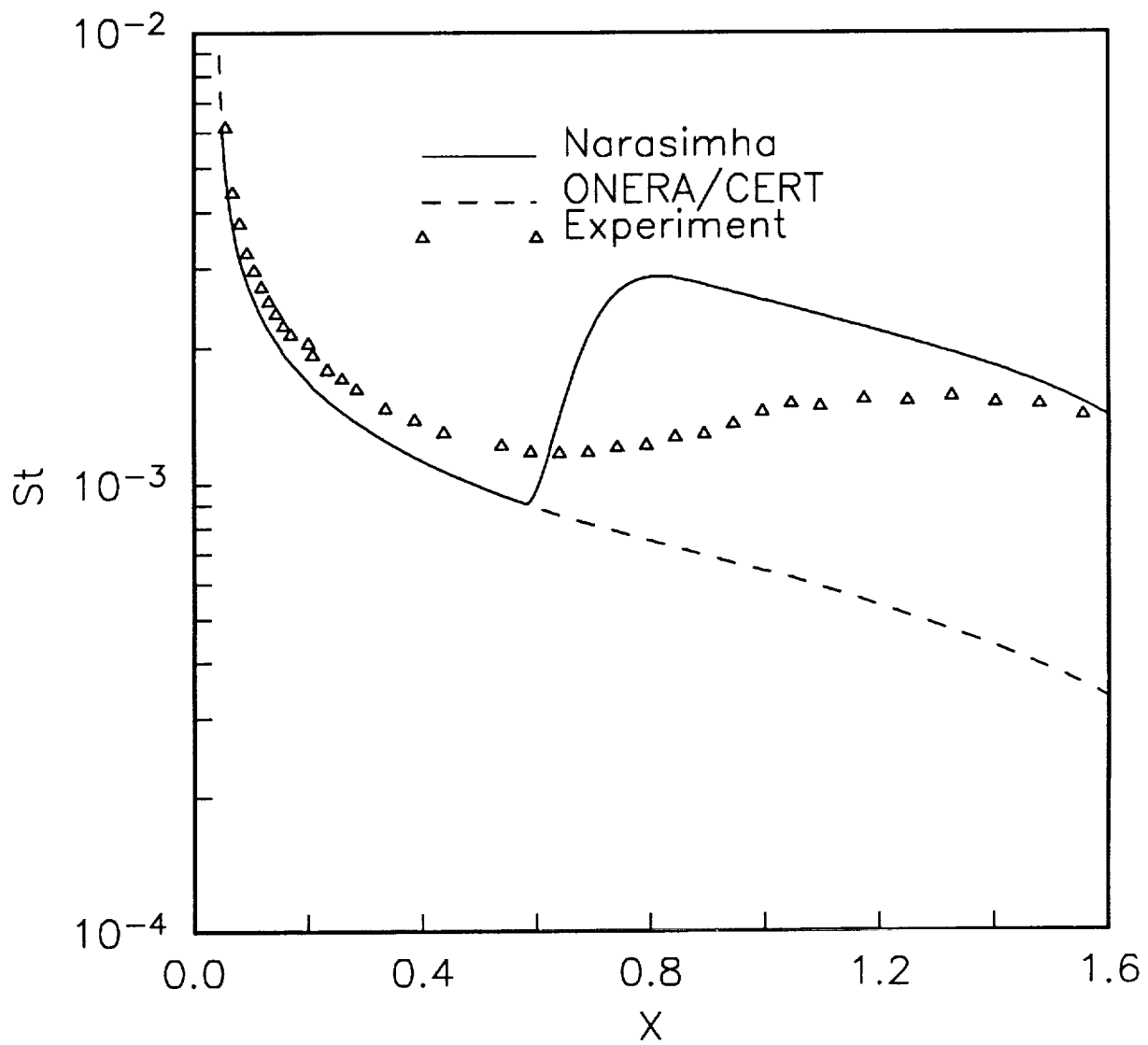
Figure 7(b). Transitional flow with a strongly favorable pressure gradient (Flow 2, Case 2). Experimental data from Blair and Werle [17] and Blair (personal communication).
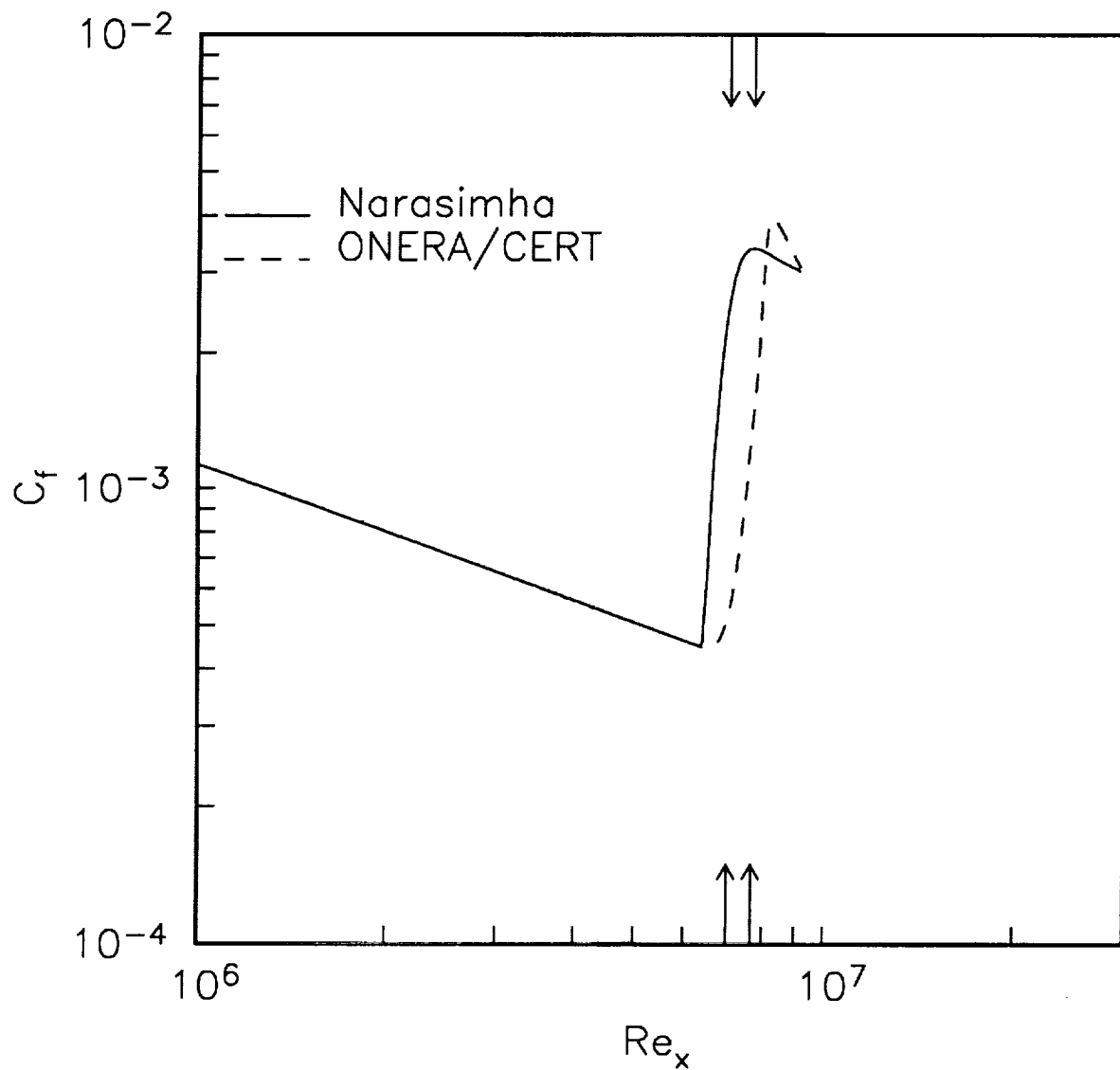
Figure 8(a). Transitional flow on a cone with $M_{ref} = 1.16$ (Flow 3, Case 1). Arrows indicate start and end of transition in experiments of Fisher and Dougherty [18].
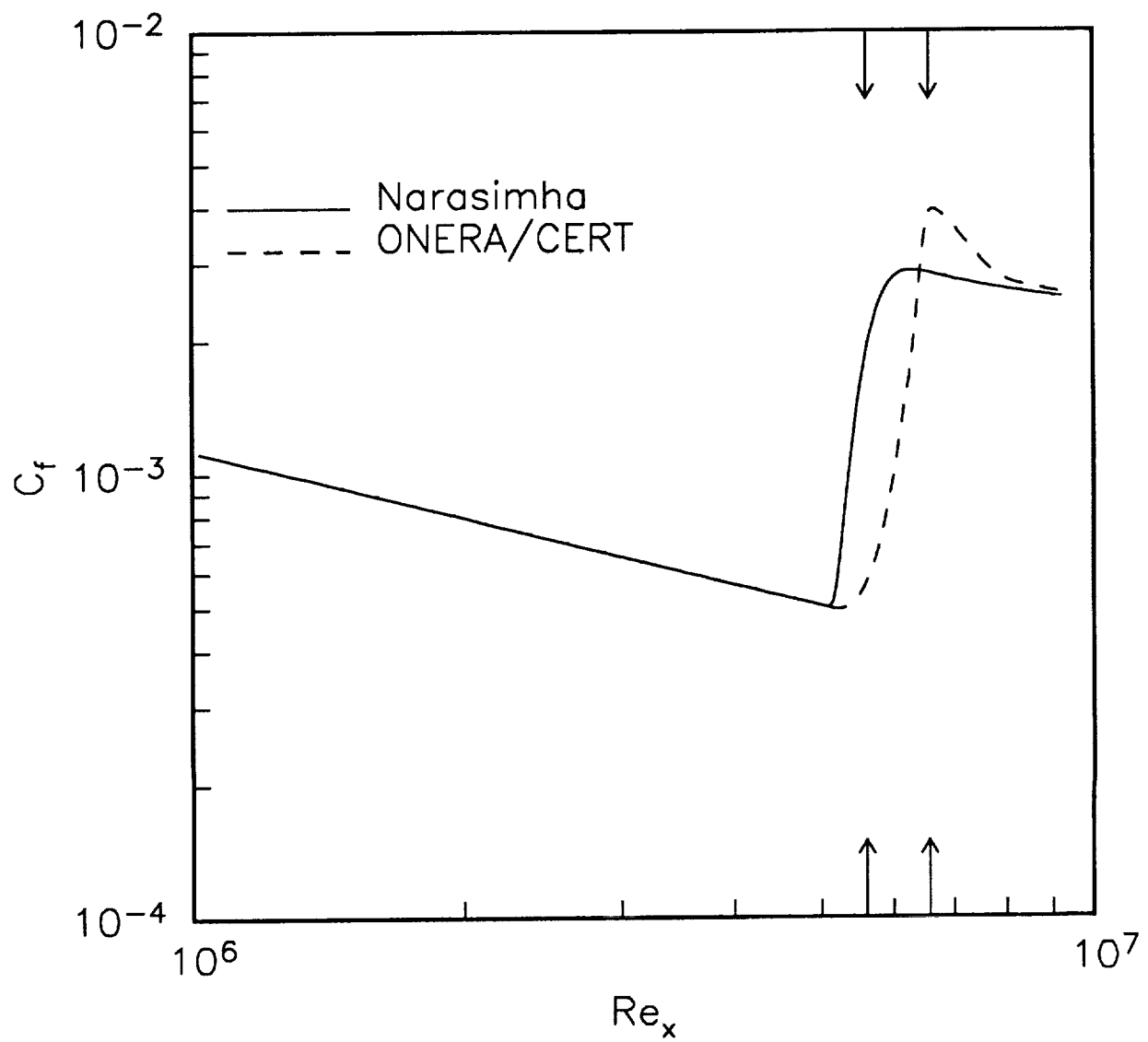
Figure 8(b). Transitional flow on a cone with M_{ref}= 1.30 (Flow 3, Case 2). Arrows indicate start and end of transition in experiments of Fisher and Dougherty [18].
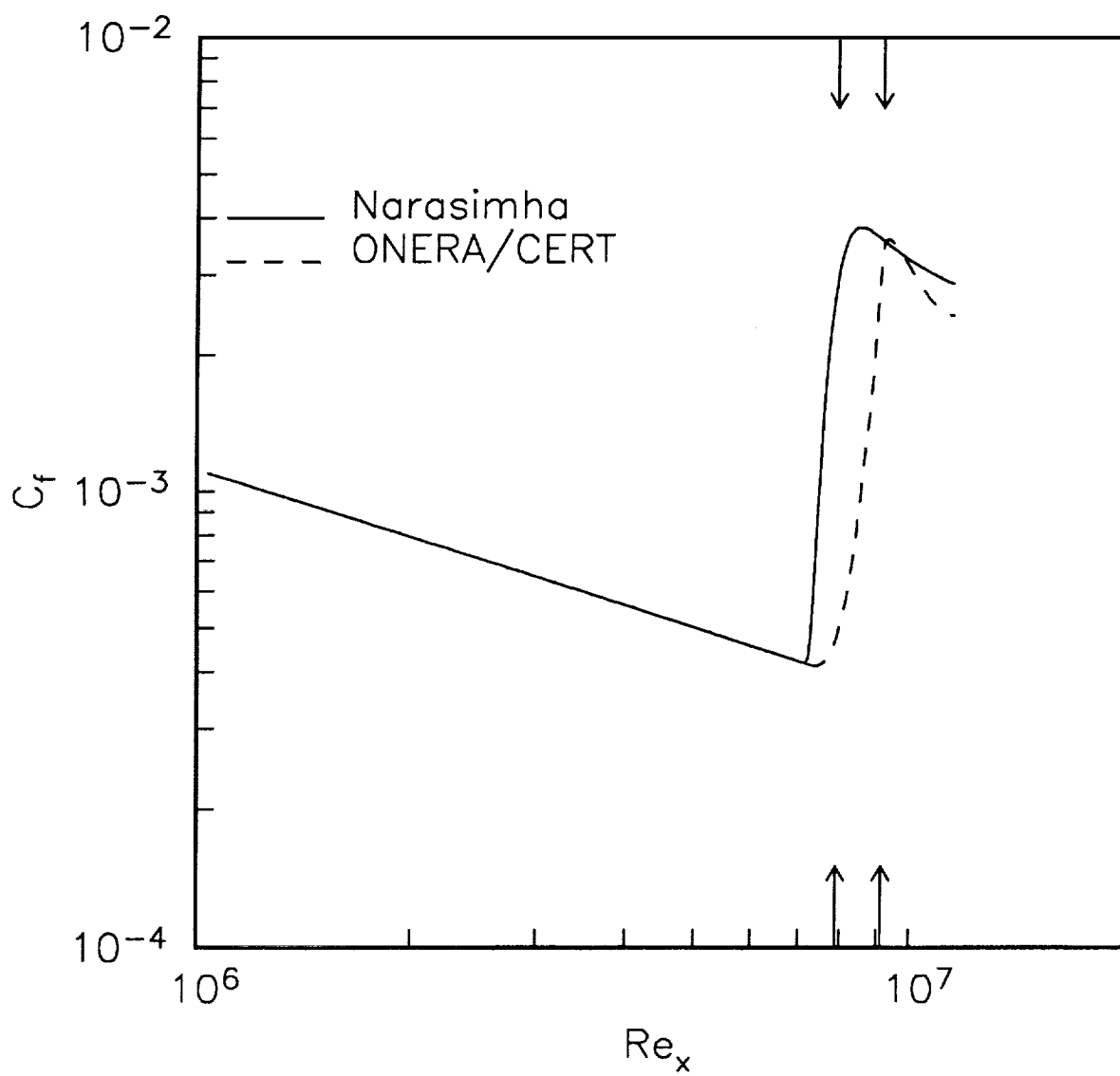
Figure 8(c). Transitional flow on a cone with $M_{ref} = 1.55$ (Flow 3, Case 3). Arrows indicate start and end of transition in experiments of Fisher and Dougherty [18].
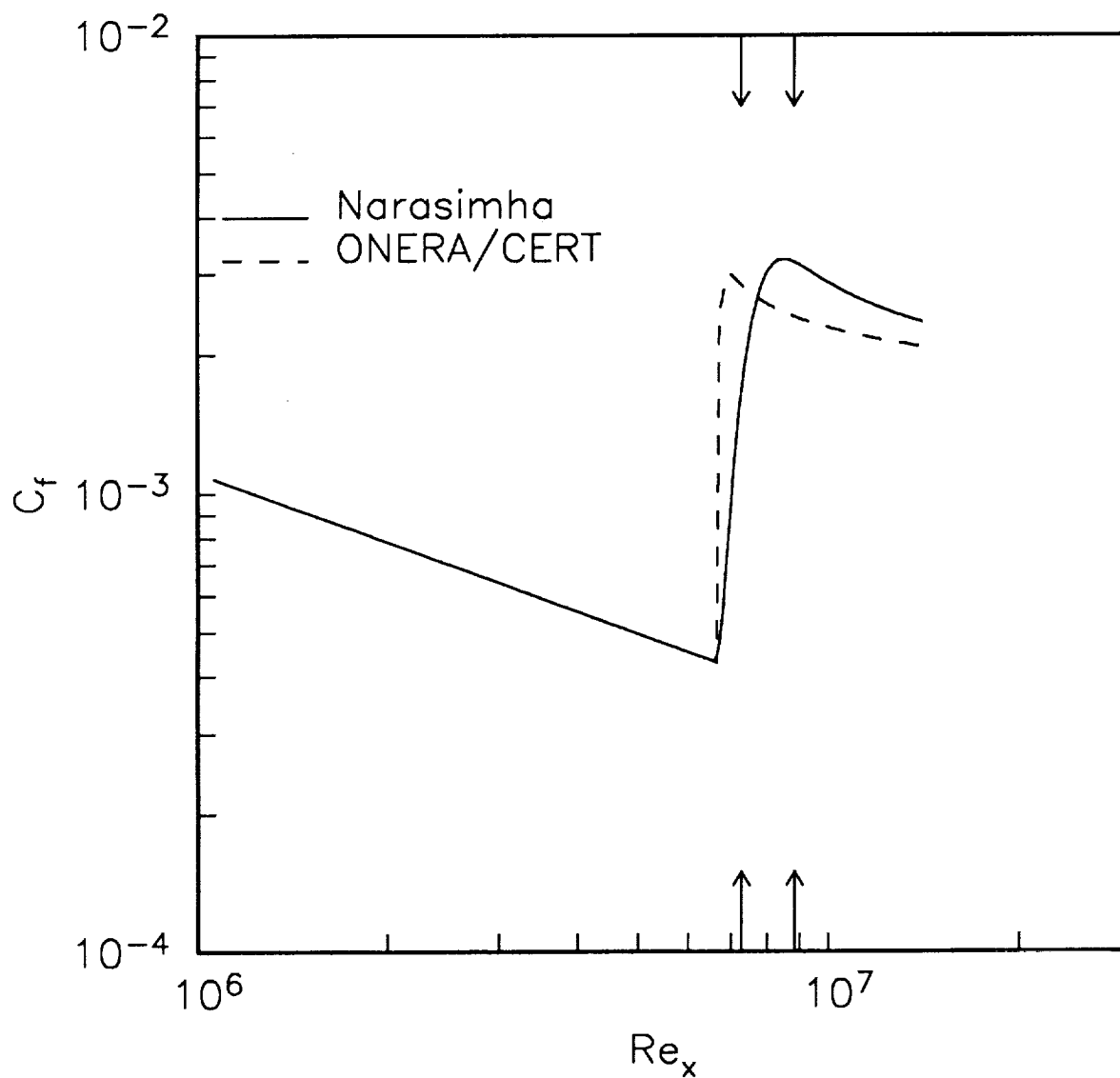
Figure 8(d). Transitional flow on a cone with $M_{ref}=$ 1.86 (Flow 3, Case 4). Arrows indicate start and end of transition in experiments of Fisher and Dougherty [18].
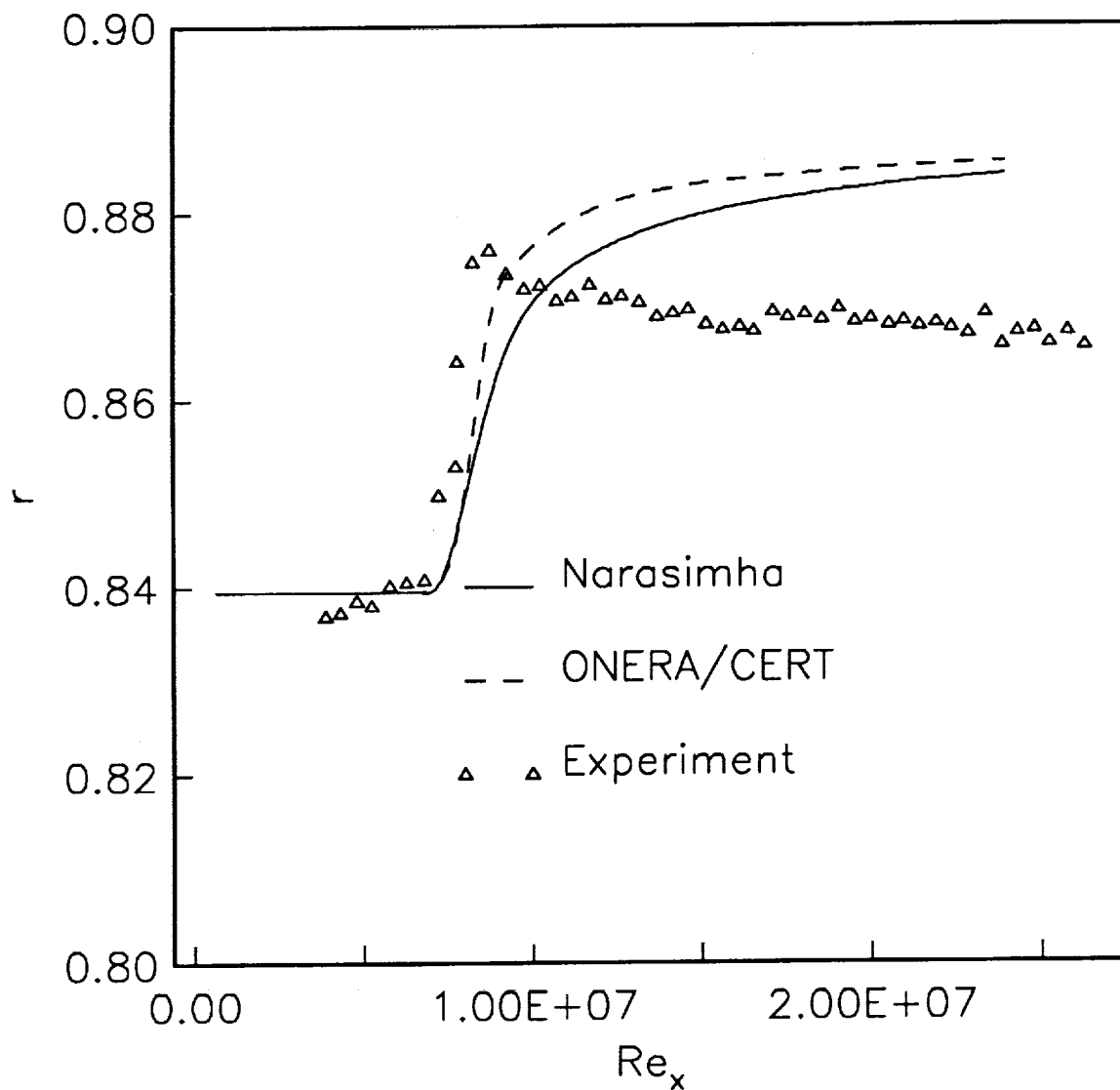
Figure 8(e). Transitional flow on a cone with M_{ref}= 3.36, P_{ref}=2.23x10^4 Pa, (Flow 3, Case 5). Experimental data of Chen, Malik and Beckwith [20].
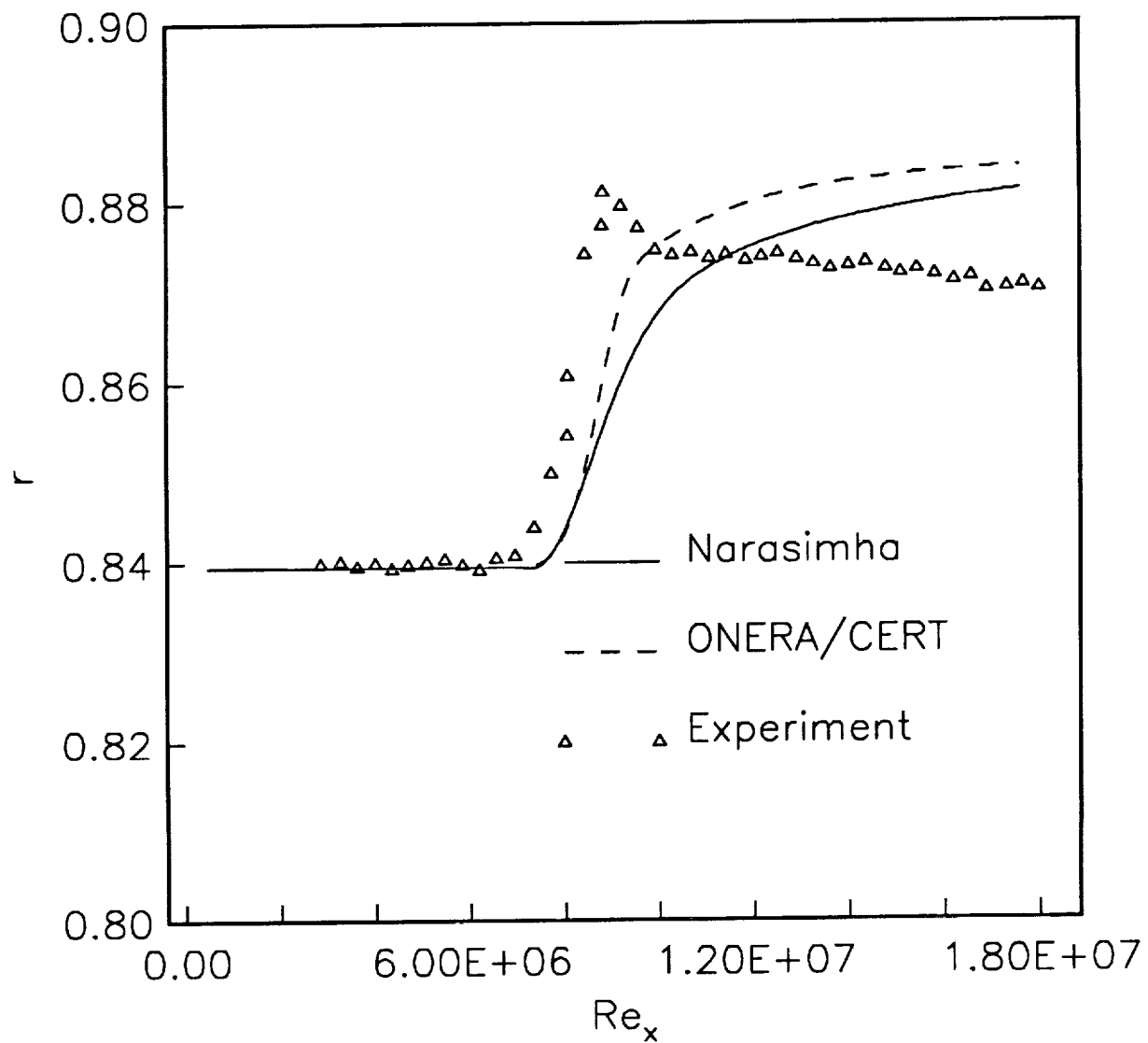
Figure 8(f). Transitional flow on a cone with M_{ref}= 3.36, P_{ref}=1.69x10^4 Pa, (Flow 3, Case 6). Experimental data of Chen, Malik and Beckwith [20].
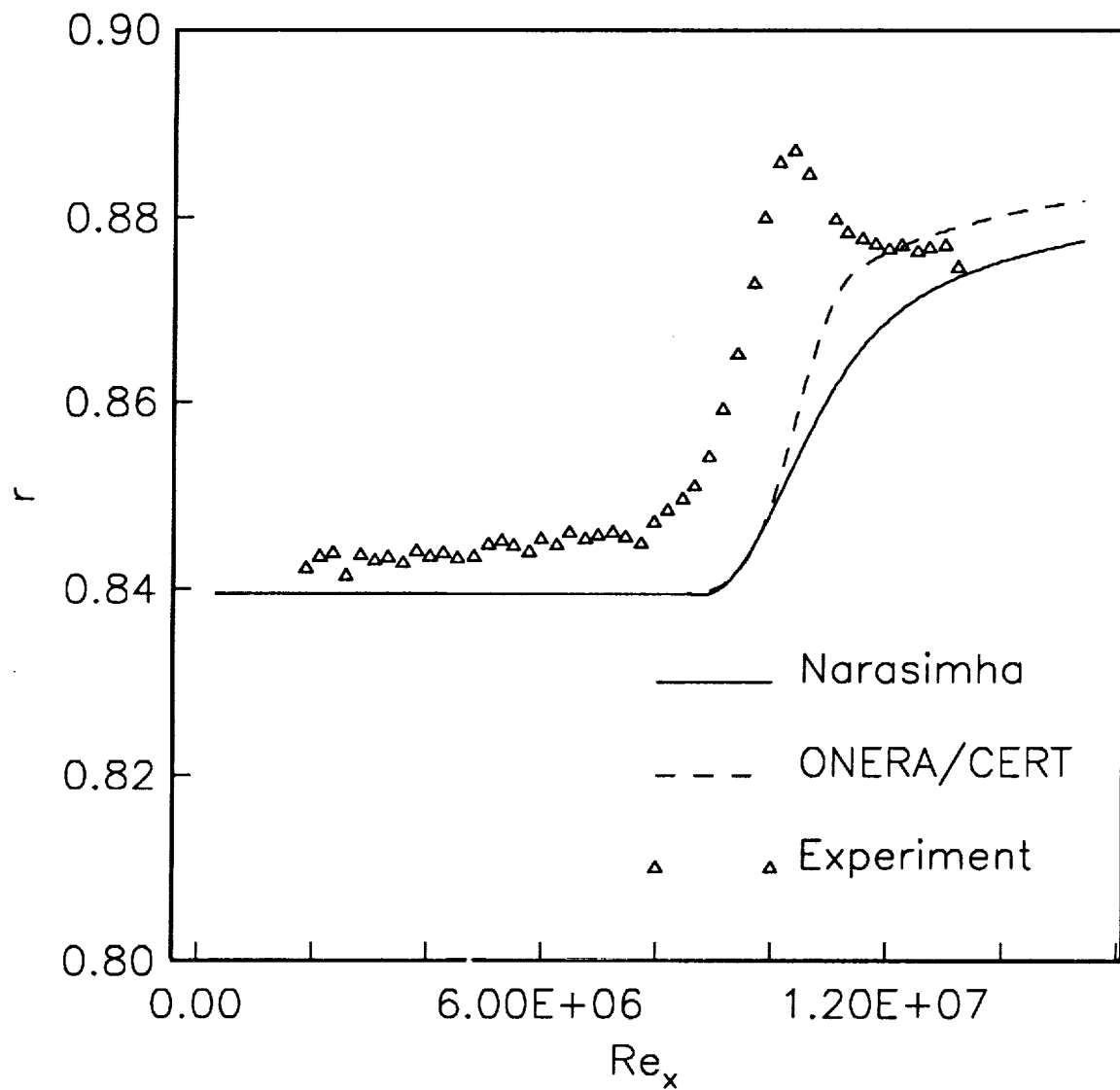
Figure 8(g). Transitional flow on a cone with M_{ref}= 3.36, P_{ref}=1.10x10^4 Pa, (Flow 3, Case 7). Experimental data of Chen, Malik and Beckwith [20].
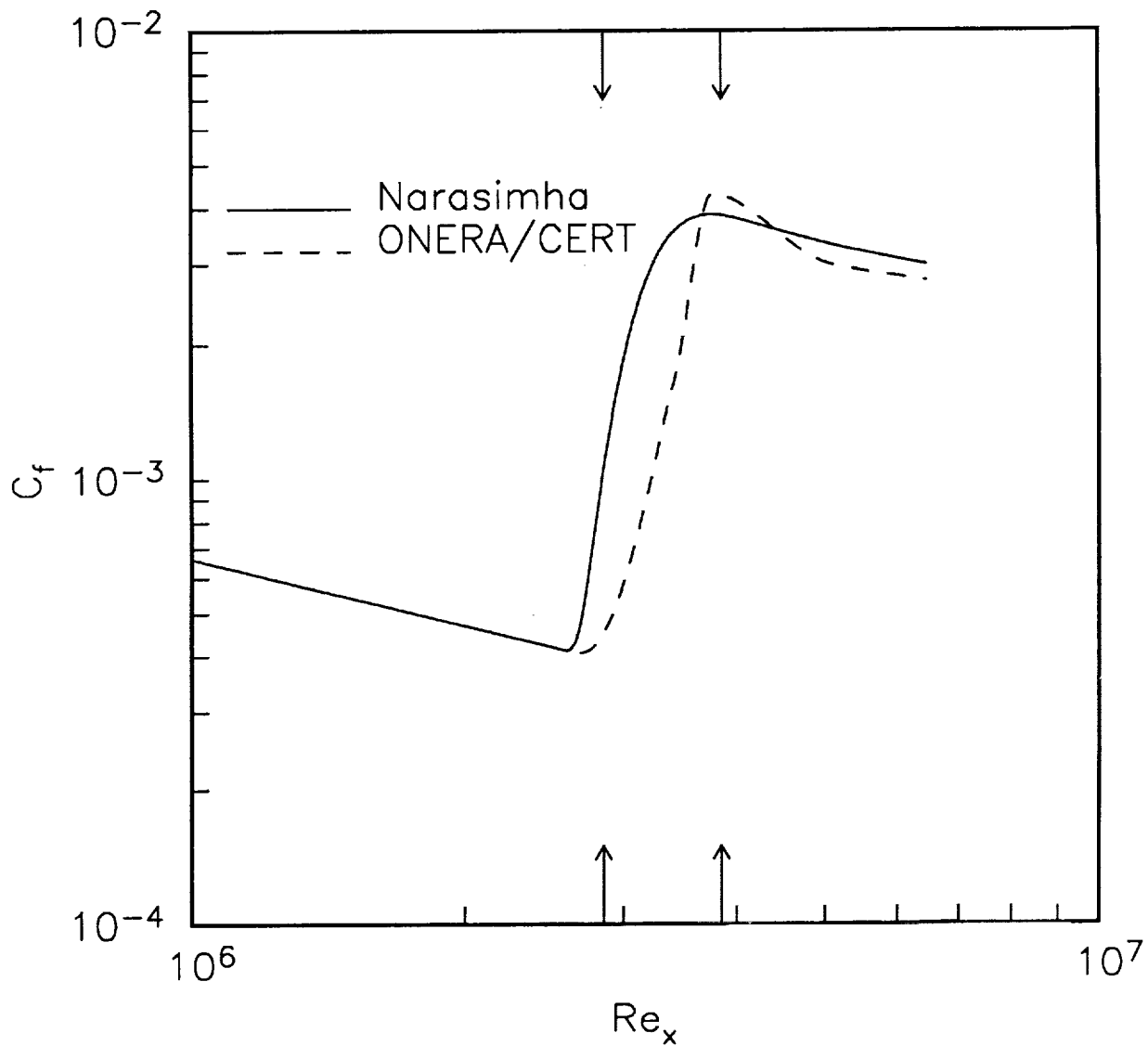
Figure 9(a). Transitional flow with a zero pressure gradient with free−stream−turbulence level 0.042% (Flow 4, Case 1). Arrows indicate the start and end of transition in experiments of Schubauer and Skramstad [23].
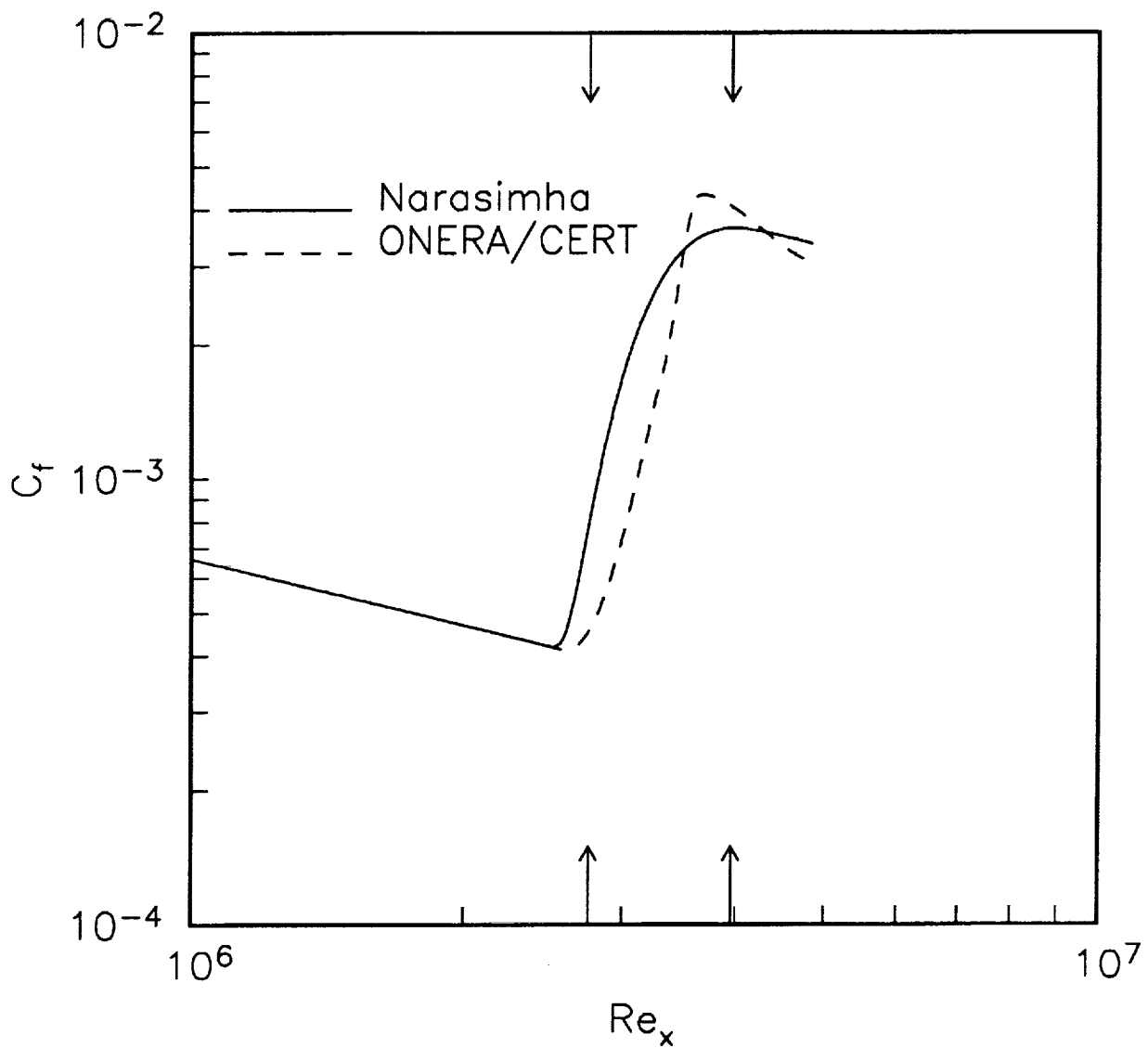
Figure 9(b). Transitional flow with a zero pressure gradient with free—stream—turbulence level 0.10% (Flow 4, Case 2). Arrows indicate the start and end of transition in experiments of Schubauer and Skramstad [23].

64
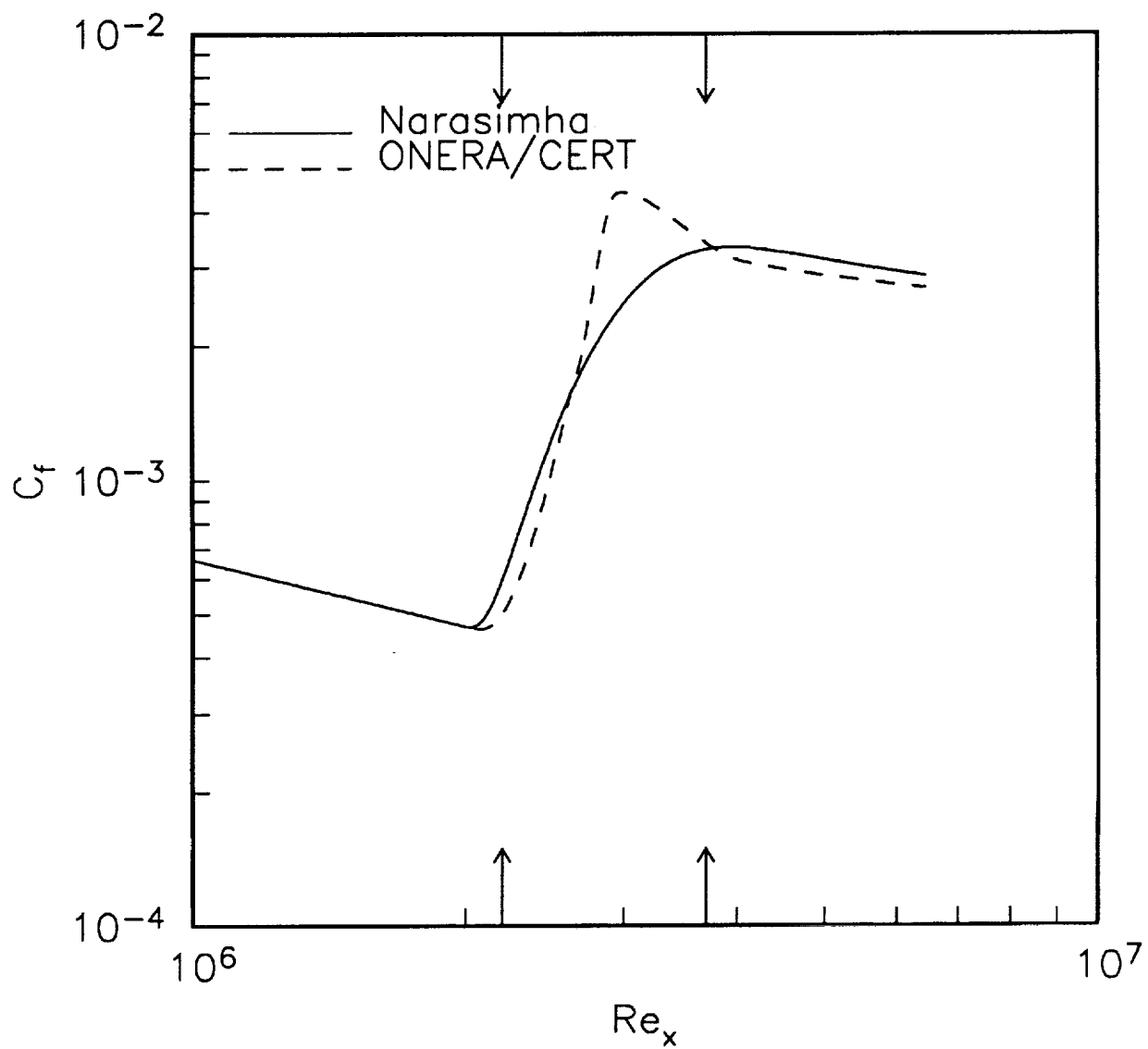
Figure 9(c). Transitional flow with a zero pressure gradient with free−stream−turbulence level 0.20% (Flow 4, Case 3). Arrows indicate the start and end of transition in experiments of Schubauer and Skramstad [23].
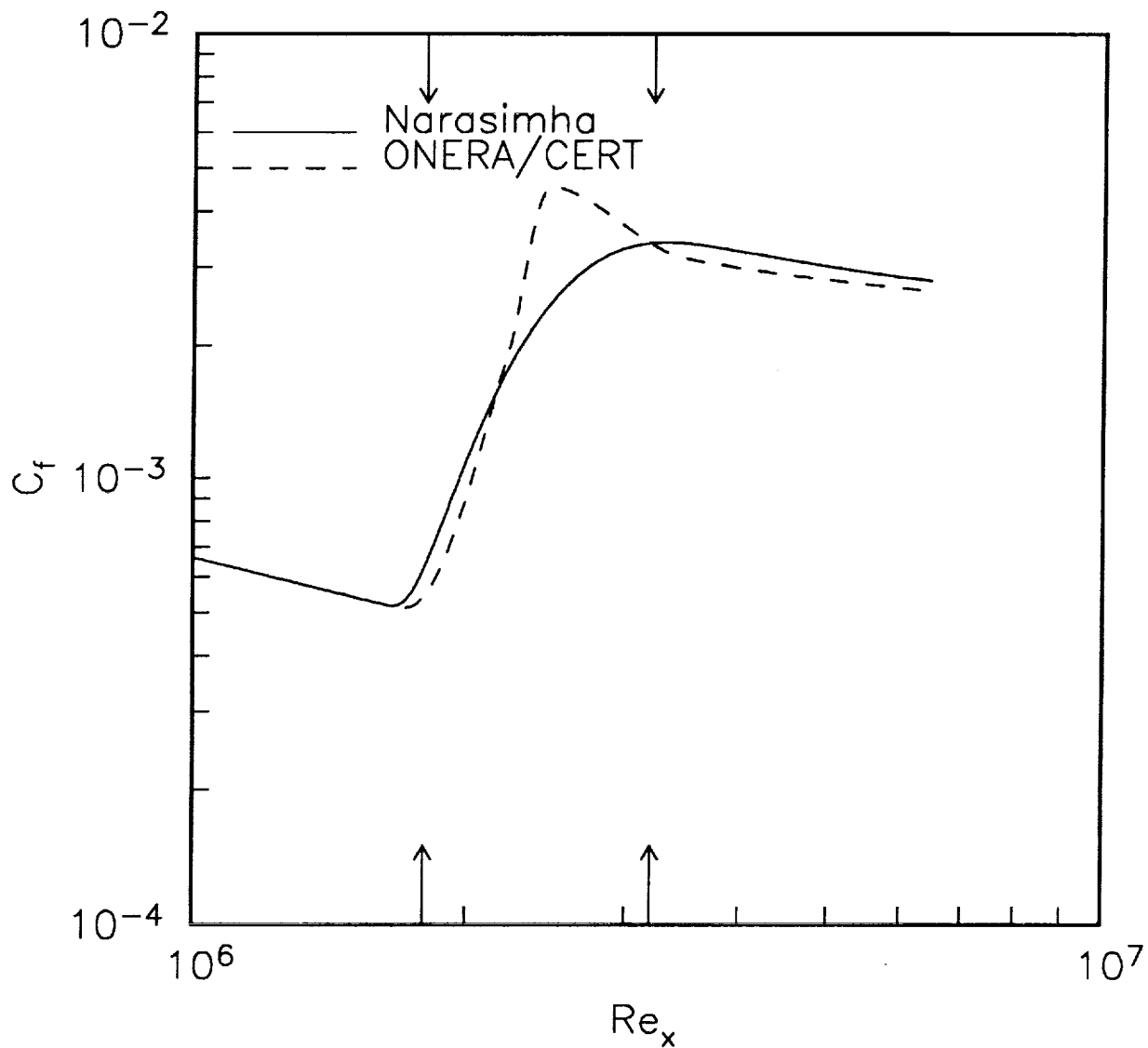
Figure 9(d). Transitional flow with a zero pressure gradient with free-stream-turbulence level 0.26% (Flow 4, Case 4). Arrows indicate the start and end of transition in experiments of Schubauer and Skramstad [23].
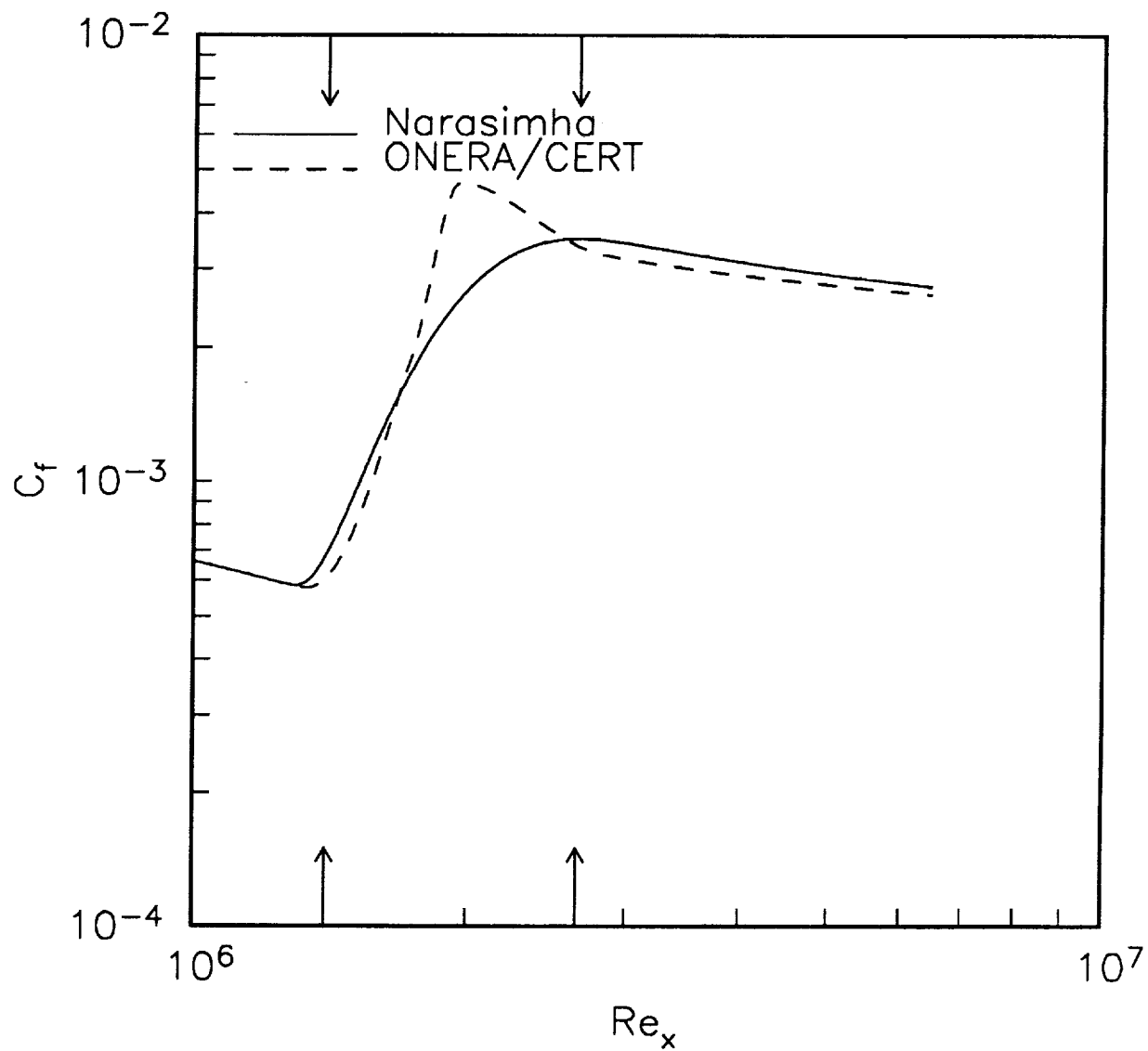
Figure 9(e). Transitional flow with a zero pressure gradient
with free-stream-turbulence level 0.34% (Flow 4,
Case 5). Arrows indicate the start and end of
transition in experiments of Schubauer and
Skramstad [23].
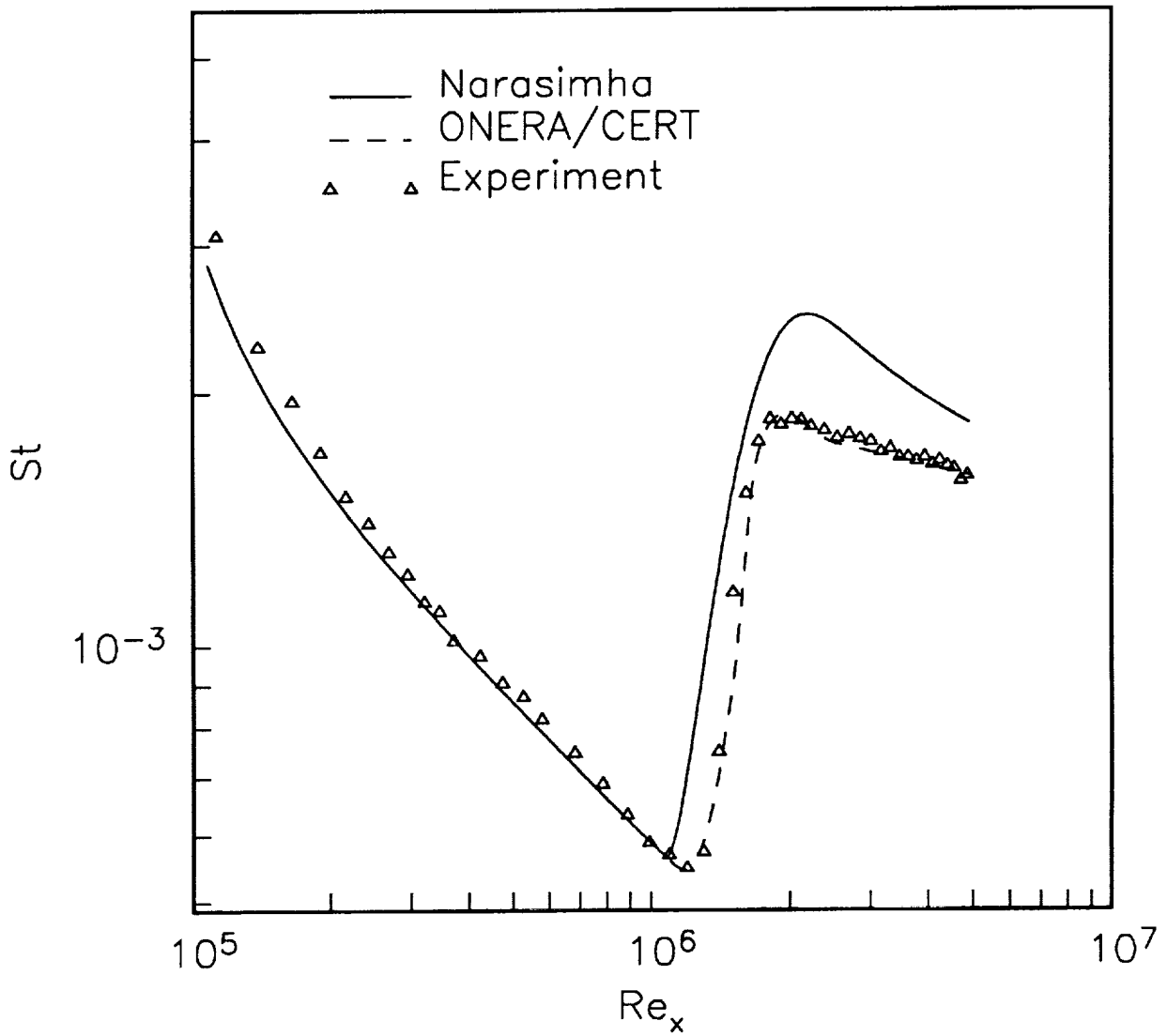
Figure 9(f). Transitional flow on a heated flat plate with free-stream-turbulence level 0.25% (Flow 4, Case 6). Experimental data from Blair [17] and Blair (personal communication).
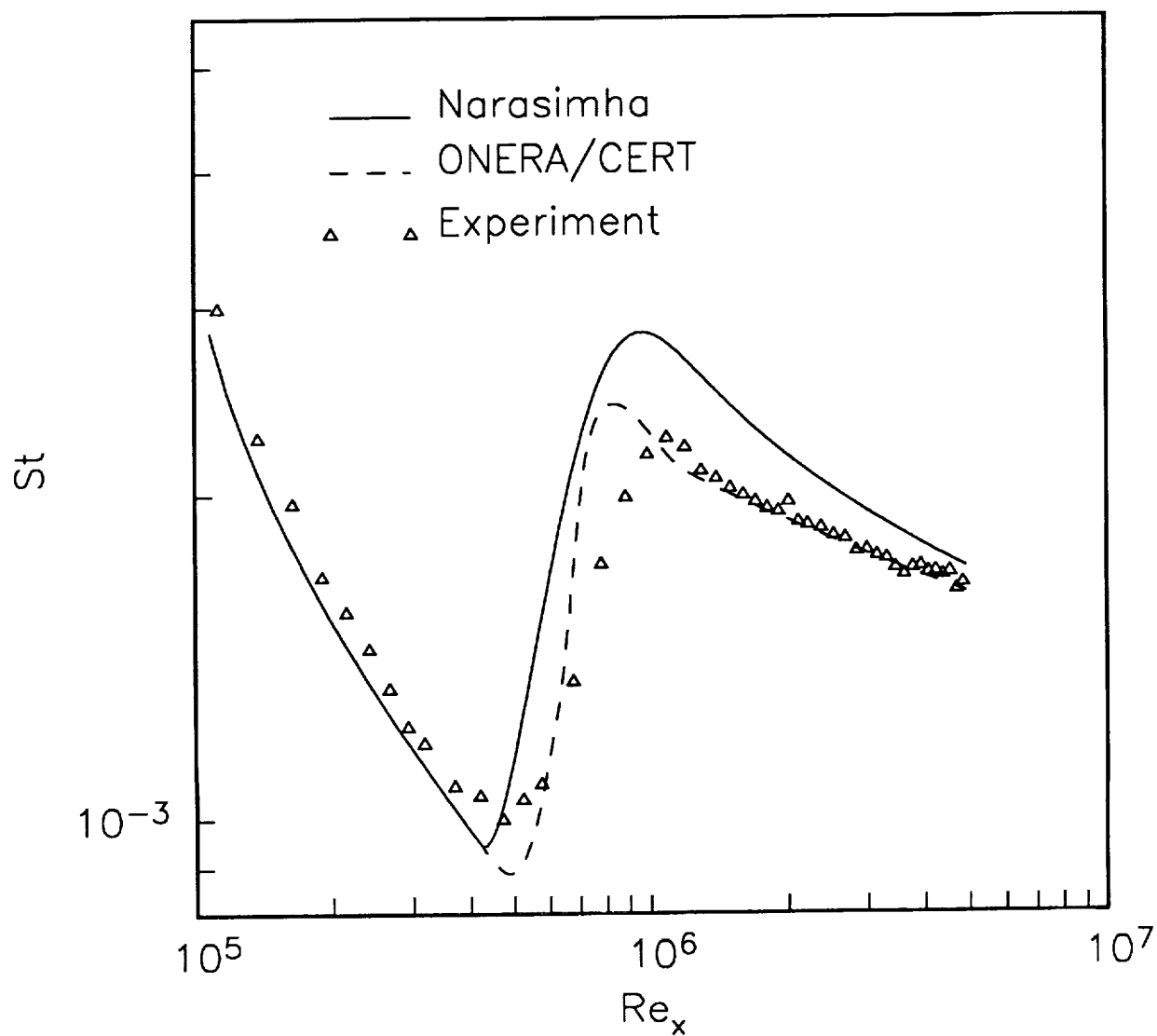
Figure 9(g). Transitional flow on a heated flat plate with free-stream-turbulence level 1.0% (Flow 4, Case 7). Experimental data from Blair [17] and Blair (personal communication).
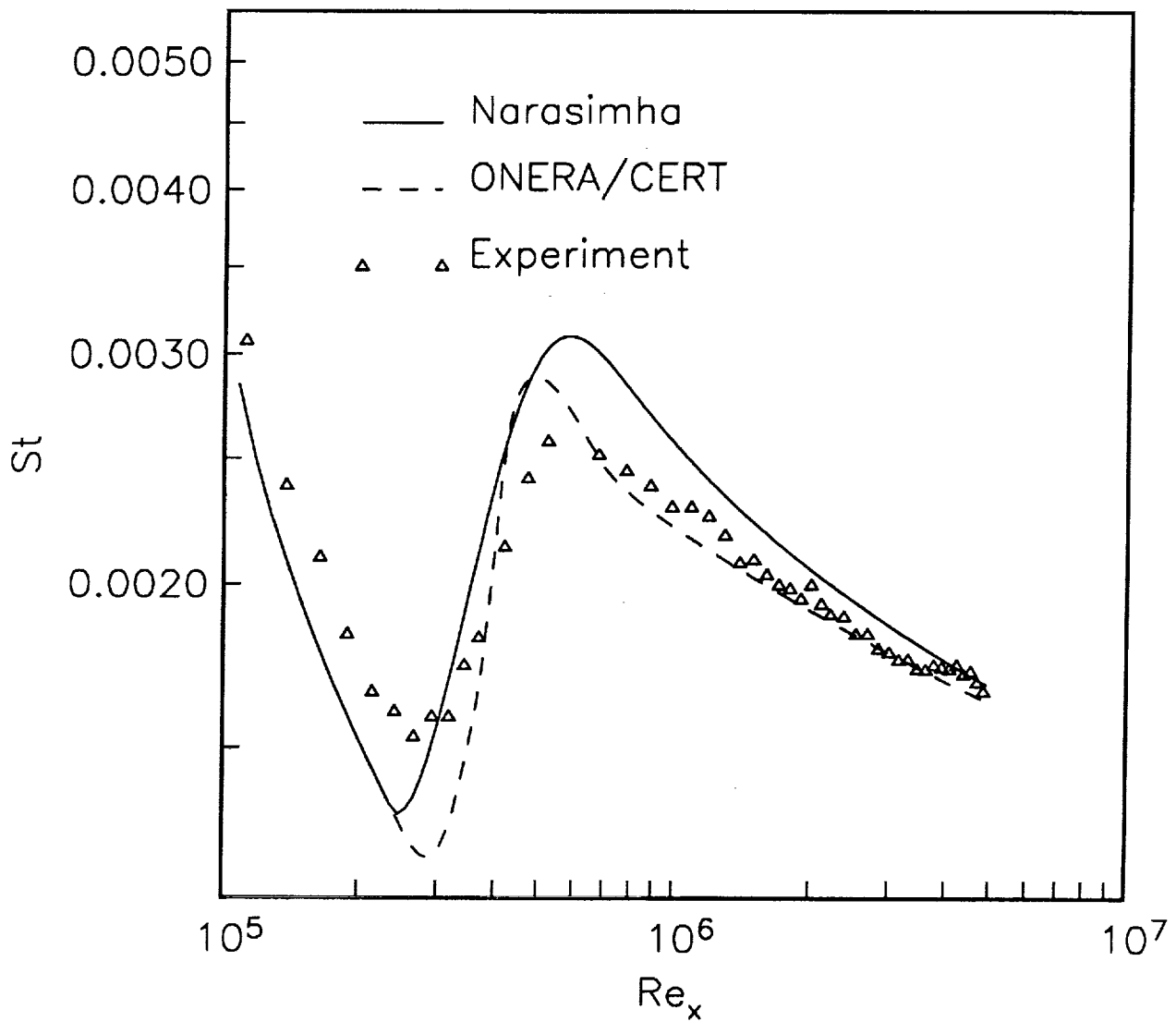
Figure 9(h). Transitional flow on a heated flat plate with free—stream—turbulence level 2.0% (Flow 4, Case 8). Experimental data from Blair [17] and Blair (personal communication).
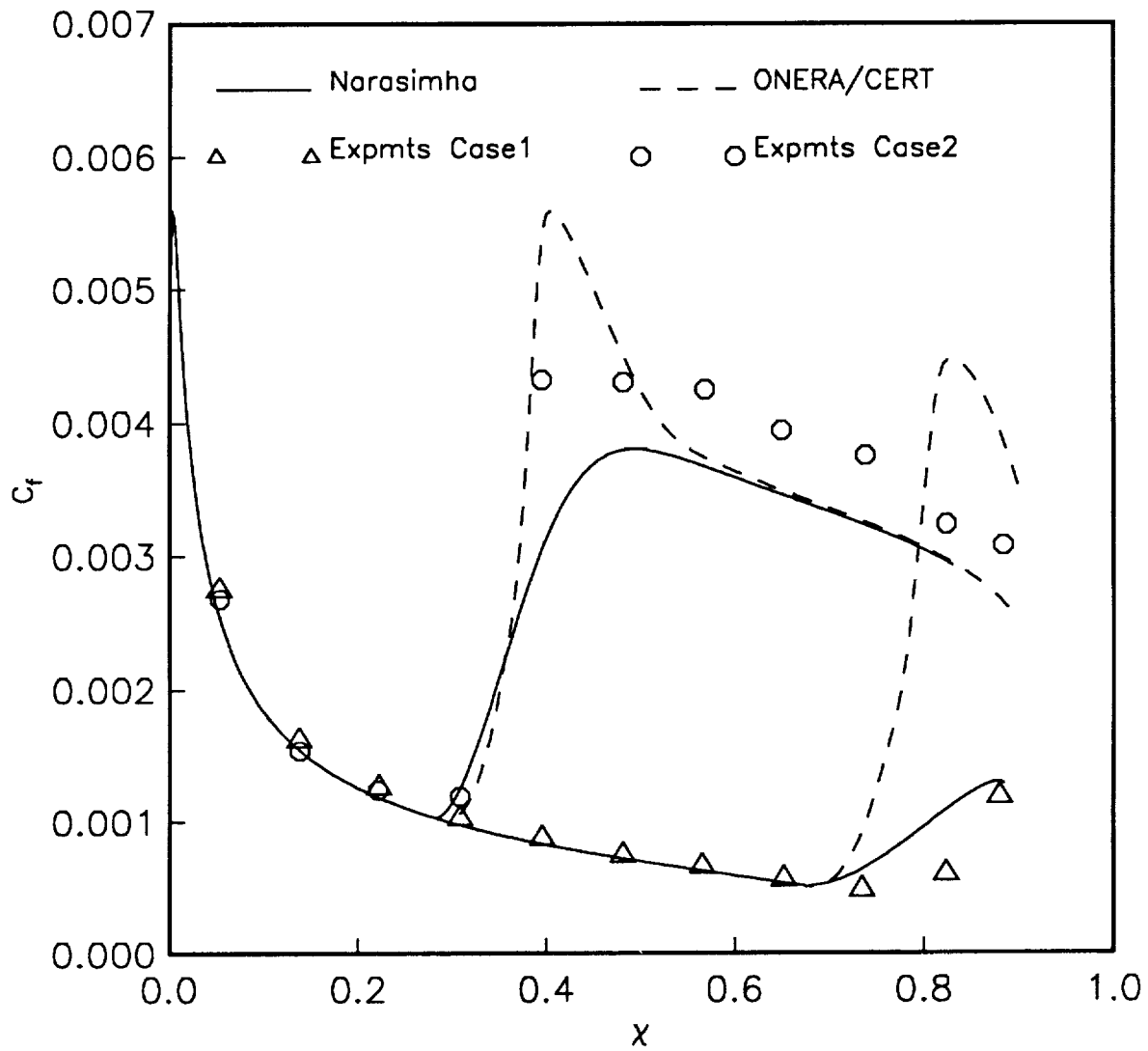
Figure 10(a). Transitional flow on a prolate spheroid with $U_\infty = 20$ m/s (Flow 5, Cases 1, no roughness strip, and 2, with roughness strip). Experimental data of Meier, Kreplin and Ming [25] and Kreplin (personal communication).
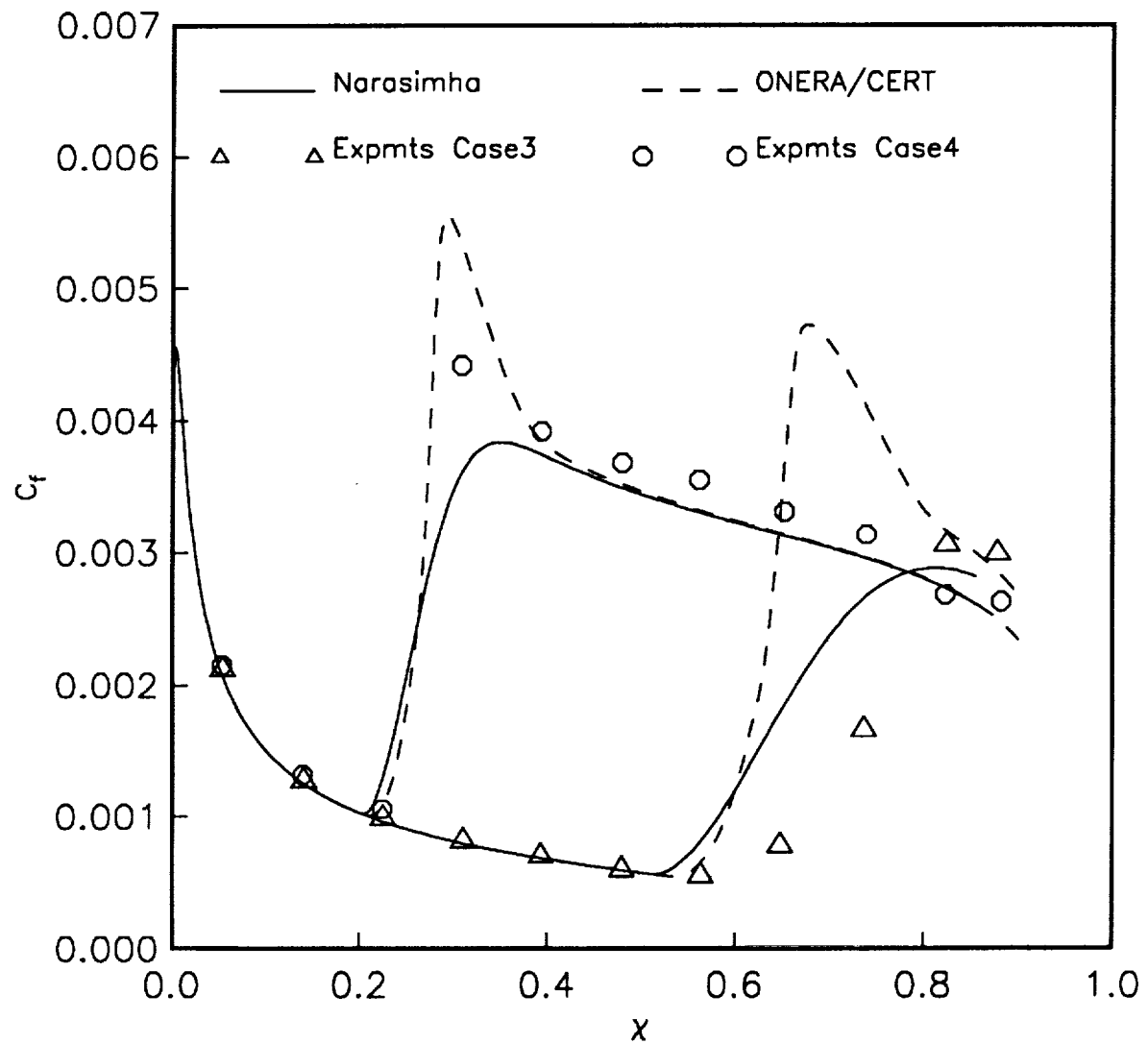
Figure 10(b). Transitional flow on a prolate spheroid with
U_∞ = 30 m/s (Flow 5, Cases 3, no
roughness strip, and 4, with roughness strip).
Experimental data of Meier, Kreplin and Ming [25]
and Kreplin (personal communication).
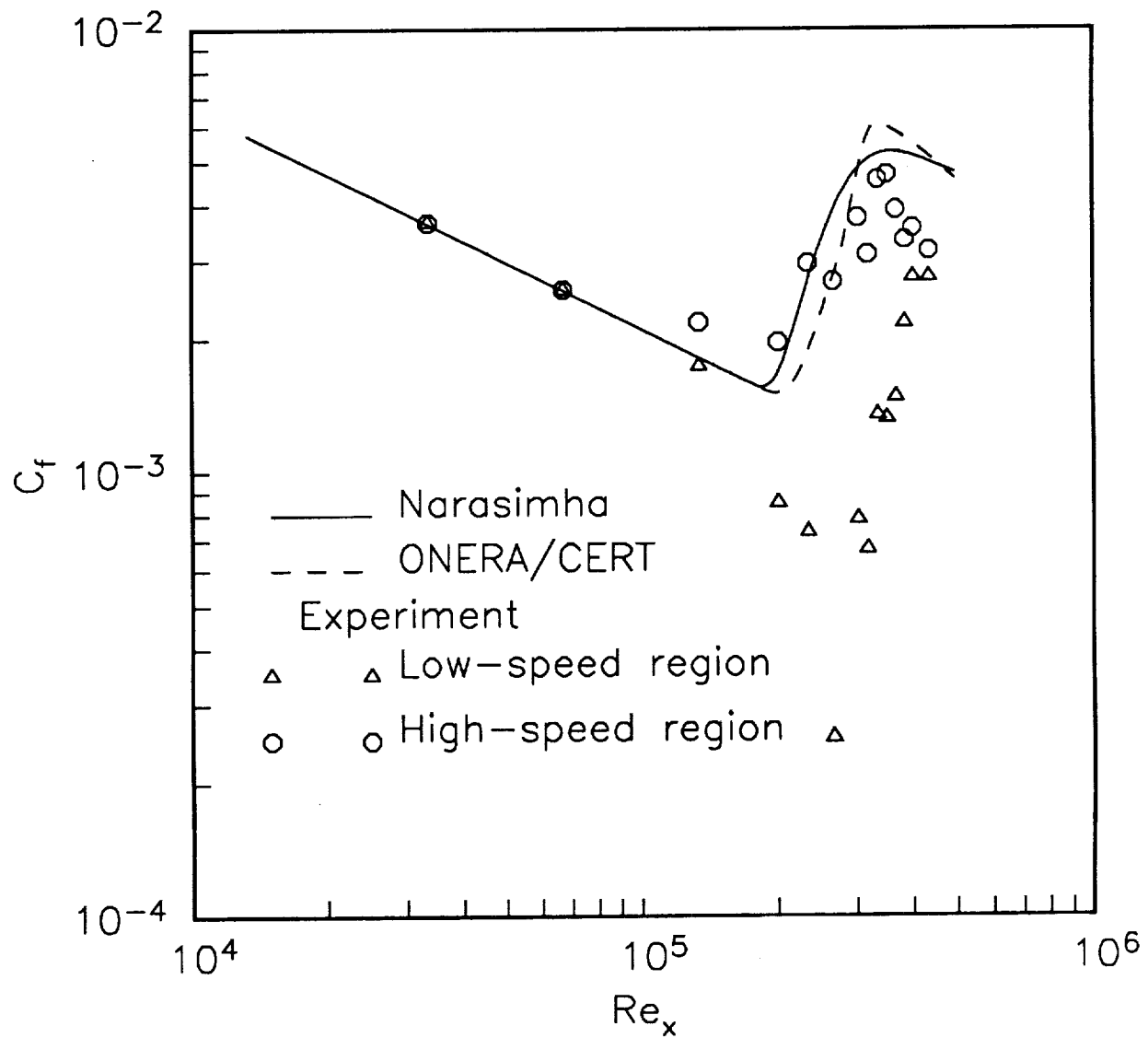
Figure 11. Transitional flow on a curved plate (Flow 6). Experimental data from Swearingen and Blackwelder [26] and Swearingen (personal communication).
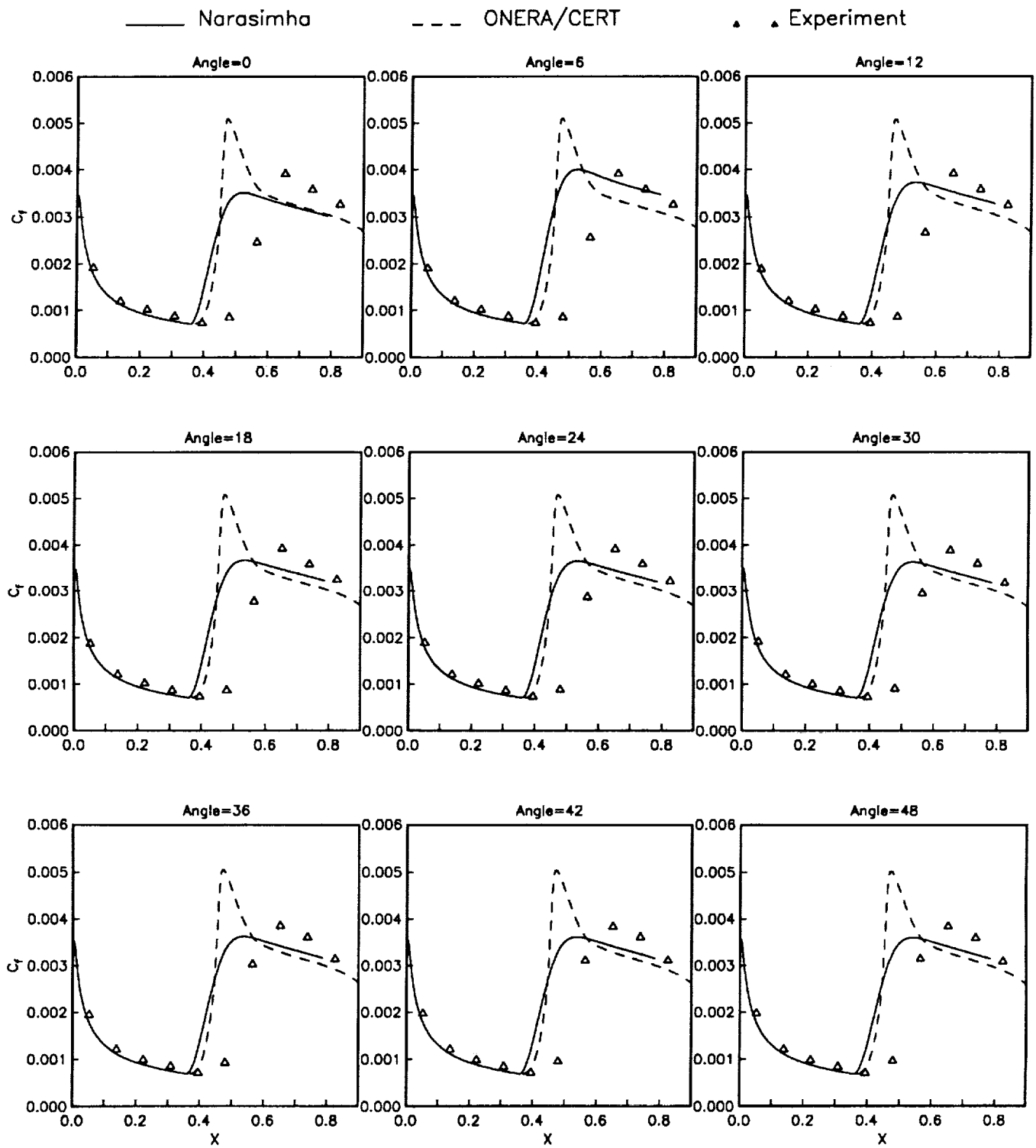
Figure 12(a). Transitional flow on a prolate spheroid at 2.5 degrees angle-of-attack and U_∞ = 45 m/s shown at different azimuthal angles (Flow7, Case 1). Experiments are from Meier and Kreplin [27] with additional data from Kreplin (personal communication).
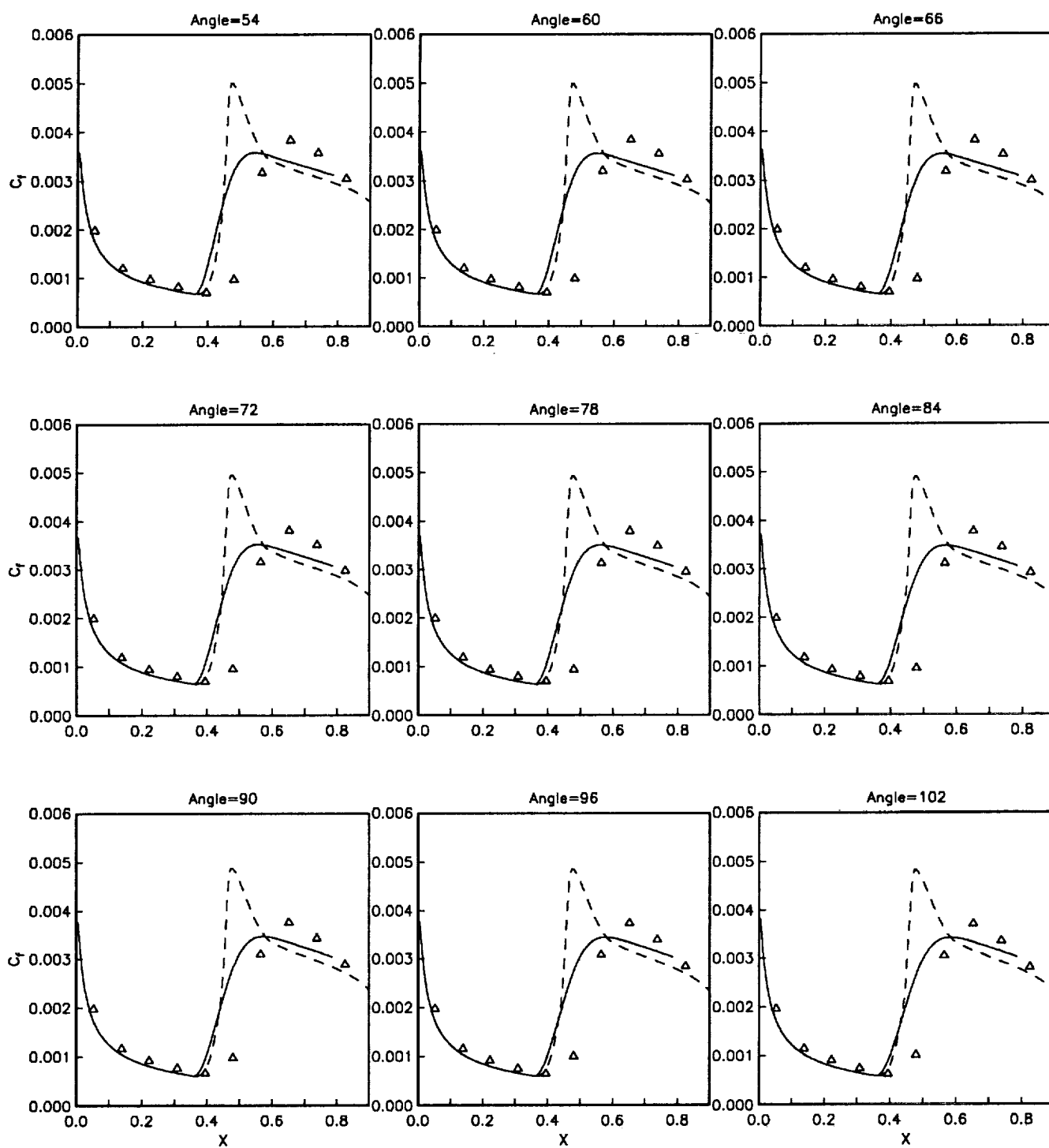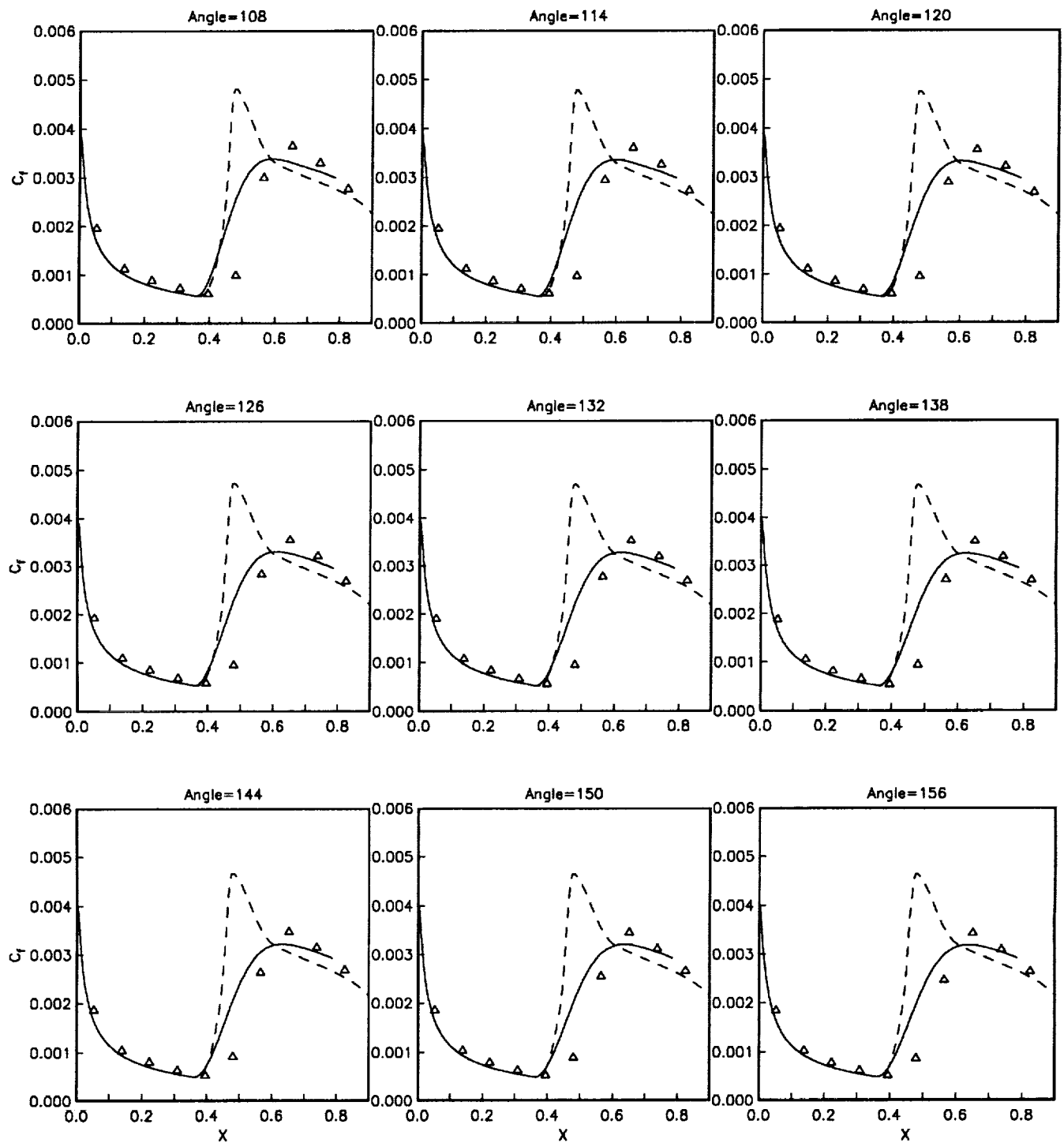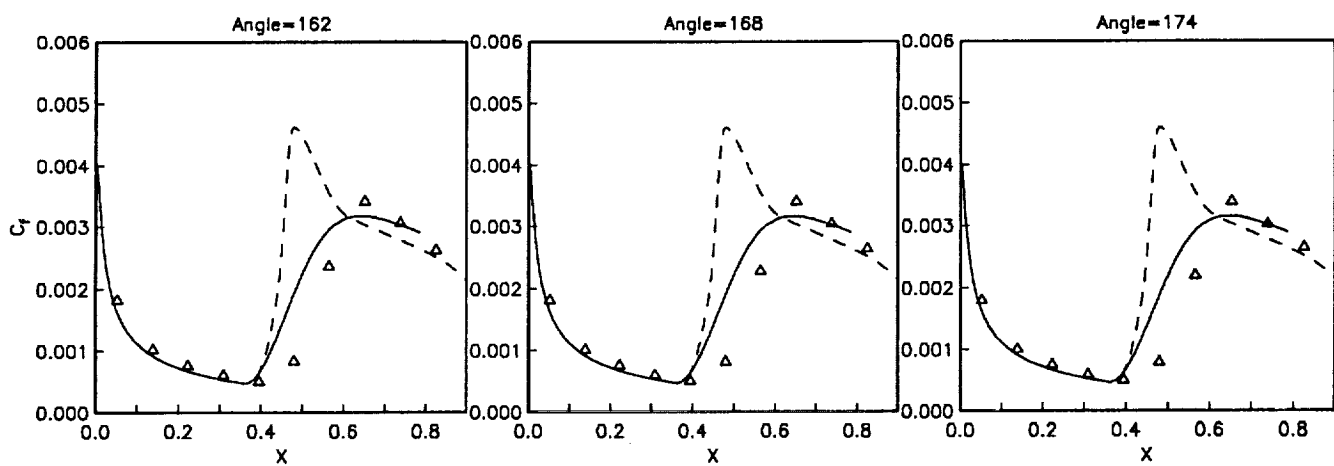
Figure 12(a). Continued

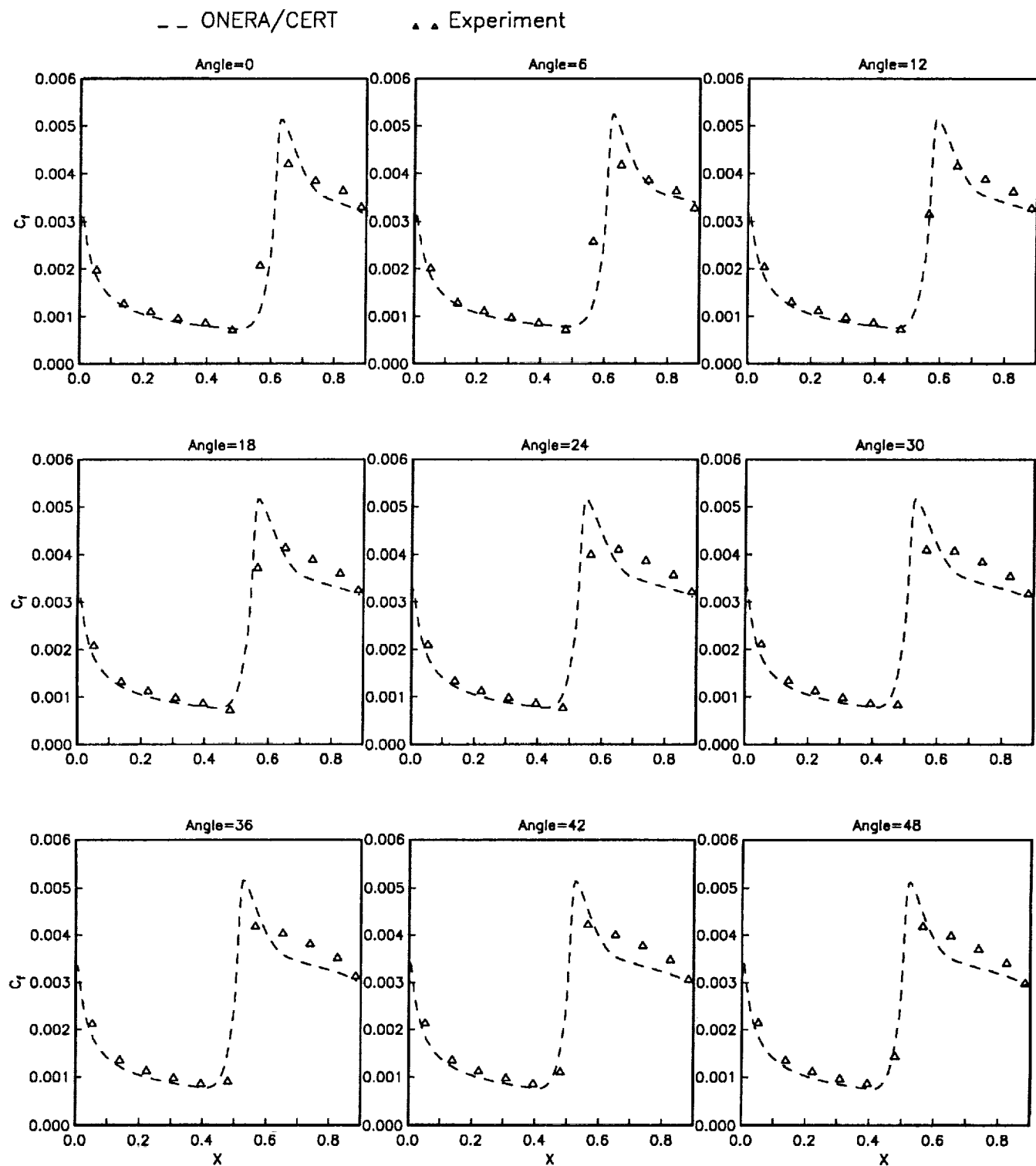Figure 12(a). Continued

Figure 12(a). Concluded.

Figure 12(b). Transitional flow on a prolate spheroid at 5.0 degrees angle-of-attack and U_∞ = 45 m/s shown at different azimuthal angles (Flow7, Case 2). Experiments are from Meier and Kreplin [27] with additional data from Kreplin, Vollmers and Meier [28].
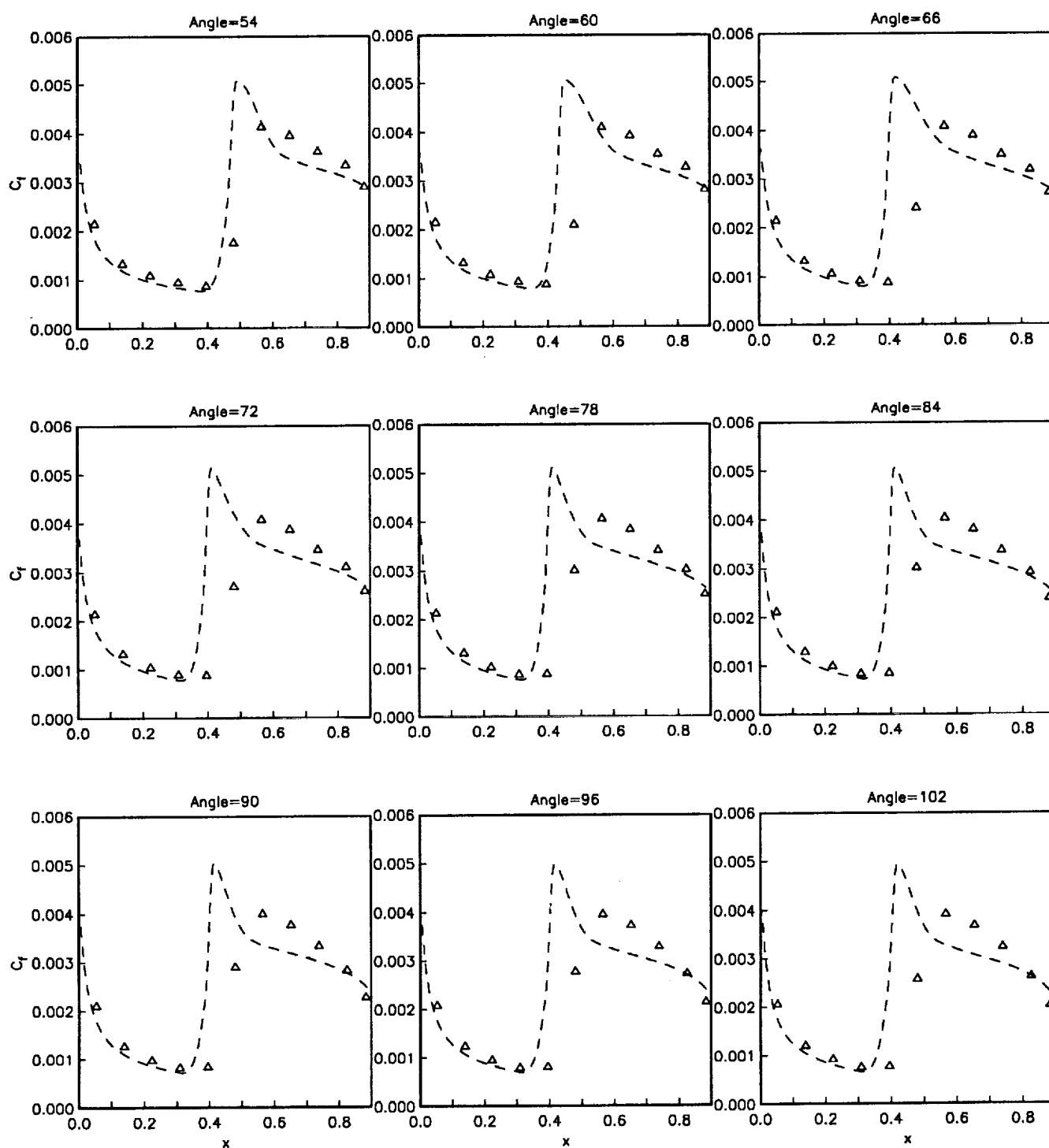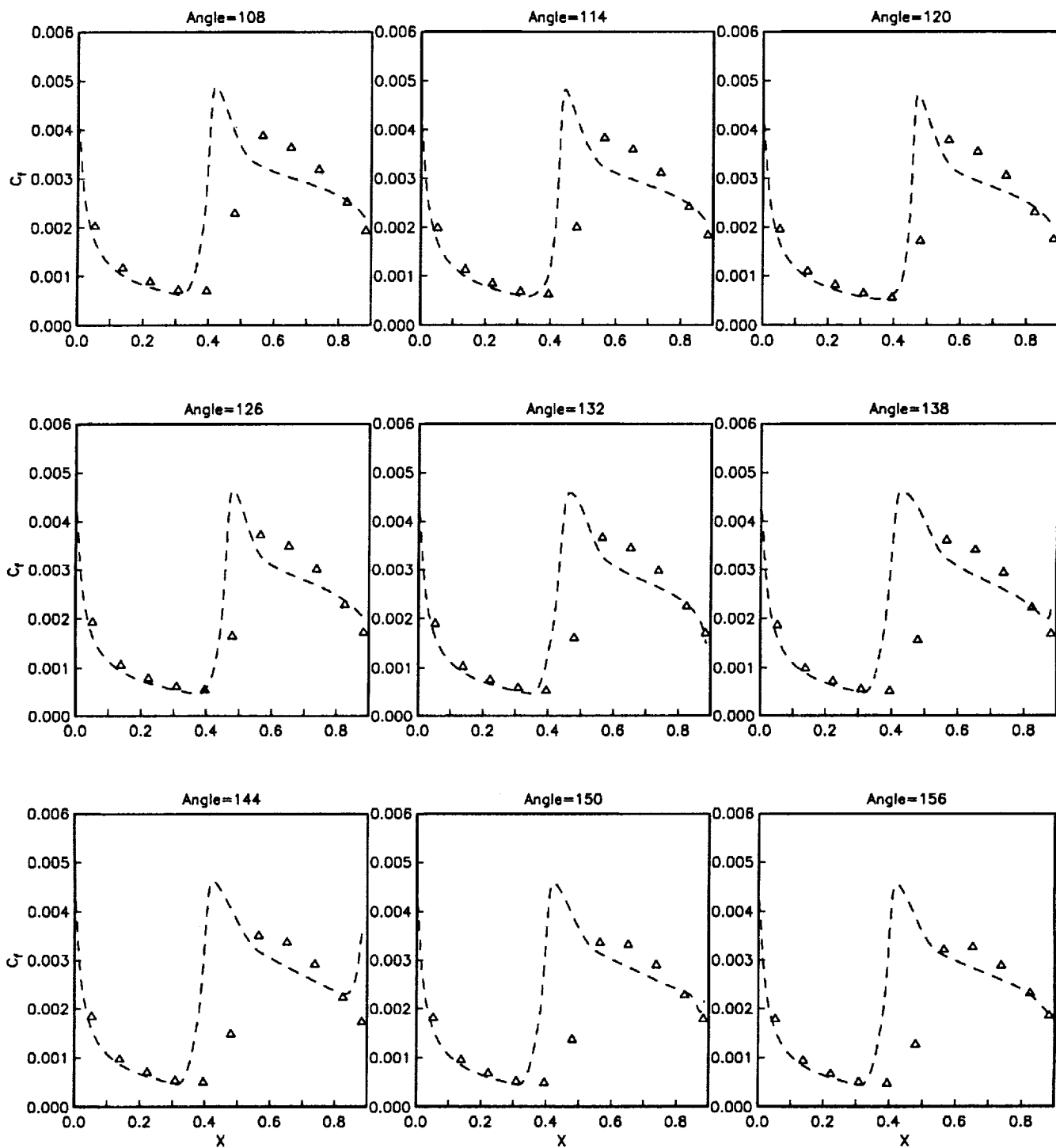
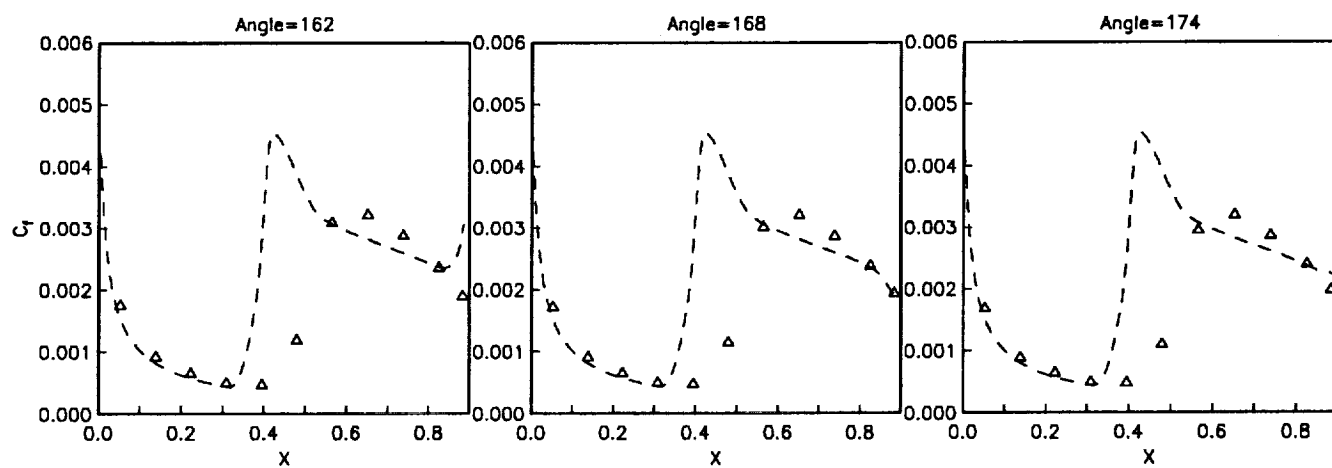Figure 12(b). Continued

79

Figure 12(b). Continued

Figure 12(b). Concluded.

Report Documentation Page

Space Administration

1. Report No. NASA CR-4371	2. Government Accession No.	3. Recipient's Catalog No.
4. Title and Subtitle Testing of Transition-Region Models: Test Cases and Data		5. Report Date May 1991
		6. Performing Organization Code
7. Author(s) Bart A. Singer (HTC), Surya P. G. Dinavahi (AS&M), and Venkit Iyer (Vigyan)		8. Performing Organization Report No.
		10. Work Unit No. 505-62-40-07
9. Performing Organization Name and Address High Technology Corp. (HTC), Mail Stop 922 Analytical Services & Materials (AS&M), Mail Stop 915 Vigyan, Inc., Mail Stop 912 NASA Langley Research Center, Hampton, VA 23665-5225		11. Contract or Grant No. HTC NAS1-18240, AS&M NAS1-18599, & ViGYAN NAS1-18585
12. Sponsoring Agency Name and Address National Aeronautics and Space Administration Langley Research Center Hampton, VA 23665-5225		13. Type of Report and Period Covered Contractor Report
		14. Sponsoring Agency Code

15. Supplementary Notes

Langley Technical Monitor: Ajay Kumar

16. Abstract

Mean-flow quantities in the laminar-turbulent-transition region and in the fully turbulent region are predicted with different models incorporated into a three-dimensional boundary-layer code. The predicted quantities are compared with experimental data for a large number of different flows and the suitability of the models for each flow is evaluated.

17. Key Words (Suggested by Author(s)) laminar - turbulent transition transition modeling linear-combination model algebraic model	18. Distribution Statement unclassified-unlimited subject category 02		
19. Security Classif. (of this report) unclassified	20. Security Classif. (of this page) unclassified	21. No. of pages 81	22. Price A05

NASA FORM 1626 OCT 86

For sale by the National Technical Information Service, Springfield, Virginia 22161-2171

NASA-Langley, 1991